Received: 23 September 2021 | Revised: 19 December 2021 | Accepted: 22 December 2021

DOI: 10.1002/glia.24140

GLIA

WILEY

RESEARCH ARTICLE

Astrocyte-targeting RNA interference against mutated superoxide dismutase 1 induces motoneuron plasticity and protects fast-fatigable motor units in a mouse model of amyotrophic lateral sclerosis

Cylia Rochat[1] | Nathalie Bernard-Marissal[1,2] | Emma Källstig[1,3] | Sylvain Pradervand[4] | Florence E. Perrin[5] | Patrick Aebischer[1] | Cédric Raoul[6] | Bernard L. Schneider[1,3]

[1]Ecole Polytechnique Fédérale de Lausanne (EPFL), Brain Mind Institute, Lausanne

[2]INSERM, MMG, Aix-Marseille University, Marseille, France

[3]Bertarelli Platform for Gene Therapy, Ecole Polytechnique Fédérale de Lausanne (EPFL), Geneva

[4]Genomic Technologies Facility, University of Lausanne, Lausanne, Switzerland

[5]INSERM U1198, University of Montpellier, EPHE, Montpellier, France

[6]INM, Université Montpellier, INSERM, Montpellier, France

Correspondence
Bernard L. Schneider, Brain Mind Institute, Ecole Polytechnique Fédérale de Lausanne (EPFL), Lausanne, Switzerland.
Email: bernard.schneider@epfl.ch

Present address
Bernard L. Schneider, School of Life Sciences, EPFL, Chemin des Mines 9, Geneva, Switzerland

Funding information
E-Rare-2 (ERA-NET, FP7), Grant/Award Number: 3ER30_160673; Schweizerischer Nationalfonds zur Förderung der Wissenschaftlichen Forschung, Grant/Award Number: 310030L_156460/1

Abstract

In amyotrophic lateral sclerosis (ALS) caused by *SOD1* gene mutations, both cell-autonomous and noncell-autonomous mechanisms lead to the selective degeneration of motoneurons (MN). Here, we evaluate the therapeutic potential of gene therapy targeting mutated *SOD1* in mature astrocytes using mice expressing the mutated $SOD1^{G93A}$ protein. An AAV-gfaABC$_1$D vector encoding an artificial microRNA is used to deliver RNA interference against mutated SOD1 selectively in astrocytes. The treatment leads to the progressive rescue of neuromuscular junction occupancy, to the recovery of the compound muscle action potential in the *gastrocnemius* muscle, and significantly improves neuromuscular function. In the spinal cord, gene therapy targeting astrocytes protects a small pool of the most vulnerable fast-fatigable MN until disease end stage. In the *gastrocnemius* muscle of the treated $SOD1^{G93A}$ mice, the fast-twitch type IIB muscle fibers are preserved from atrophy. Axon collateral sprouting is observed together with muscle fiber type grouping indicative of denervation/reinnervation events. The transcriptome profiling of spinal cord MN shows changes in the expression levels of factors regulating the dynamics of microtubules. Gene therapy delivering RNA interference against mutated SOD1 in astrocytes protects fast-fatigable motor units and thereby improves neuromuscular function in ALS mice.

KEYWORDS
amyotrophic lateral sclerosis, astrocyte, gene therapy, neuromuscular function, neuronal plasticity, RNA interference, superoxide dismutase 1

1 | INTRODUCTION

Amyotrophic lateral sclerosis (ALS) is a fatal neurodegenerative disease characterized by the progressive and selective loss of motoneurons (MN) in the cortex, brainstem, and spinal cord. Whereas 90% of ALS cases are sporadic, the remaining 10% are familial (fALS). Pathogenic mutations in the gene encoding Cu/Zn superoxide dismutase (*SOD1*) are considered to cause 20% of fALS cases (Taylor et al., 2016).

Mice overexpressing mutated SOD1 (mSOD1) replicate the main features of ALS (Gurney et al., 1994). In the spinal cord, neurodegeneration follows a specific pattern, characterized by the higher vulnerability of the fast-fatigable MN, which innervate fast-twitch type IIB muscle fibers (Pun et al., 2006). Importantly, noncell-autonomous pathogenic mechanisms are also involved in MN degeneration (Beers et al., 2006; Boillee et al., 2006; Pramatarova et al., 2001). Mutated SOD1 has key pathogenic effects in glial cells including astrocytes, microglial cells and oligodendrocytes. Suppressing mSOD1 in these cell types modifies onset and/or progression of the disease (Boillee et al., 2006; Kang et al., 2013; Yamanaka et al., 2008). Furthermore, knockout of factors enhancing the neurotoxicity of astrocytes delays disease progression in the *SOD1*^{G93A} ALS mouse model (Guttenplan et al., 2020).

Diseased astrocytes have major effects on MN, both in vitro and in vivo. In co-culture systems, astrocytes derived from ALS patients or from ALS mouse models show toxic activities on MN (Aebischer et al., 2011; Haidet-Phillips et al., 2011; Nagai et al., 2007; Rojas et al., 2014). Furthermore, infusion of culture medium conditioned by primary mouse astrocytes expressing mSOD1 is sufficient to induce MN degeneration and neuromuscular dysfunction in healthy rats (Ramírez-Jarquín et al., 2017). Although the molecular cause of this toxicity remains poorly understood, some mechanisms have been proposed. Astrocytes from ALS patients and mSOD1 mice have reduced expression of *EAAT2*, which may decrease their ability to properly uptake glutamate, causing excitotoxicity in MN (Rothstein et al., 1995). Furthermore, ALS may affect the ability of astrocytes to provide essential metabolic and trophic support to MN, for instance by lowering lactate efflux (Ferraiuolo et al., 2011). Because of an abnormal ratio between pro- and mature nerve growth factor in astrocytes, the p75 signaling pathway was aberrantly upregulated in MN (Ferraiuolo et al., 2011). The release of transforming growth factor β1 (TGF-β1) is upregulated in ALS astrocytes, with possible effects on the inflammatory response and MN survival (Endo et al., 2015; Tripathi et al., 2017). Diseased astrocytes can also produce factors that are directly toxic to MN, such as high levels of NO and interferon gamma (IFNγ), which may increase oxidative stress and cause MN death (Aebischer et al., 2011; Anneser et al., 2001; Catania et al., 2001). Reactive astrocytes have also been shown to release lipocalin 2 (lcn2), which is a potent mediator of neuronal toxicity (Bi et al., 2013).

Various strategies are explored to prevent the toxic effects of diseased astrocytes in ALS, including RNA interference to lower the expression level of mSOD1 protein (Foust et al., 2013; McCampbell et al., 2018; Ralph et al., 2005; Raoul et al., 2005; Stoica et al., 2016). We previously designed an AAV9 vector combined with the gfaABC$_1$D promoter driving expression of an artificial microRNA to knockdown human SOD1 (miR SOD1) in astrocytes (Dirren et al., 2015). Following intracerebroventricular (ICV) injection in neonatal *SOD1*^{G93A} mice, this vector was found to improve the neuromuscular function and prolong animal survival. However, it remains unclear what are the effects of targeting astrocytes for gene therapy against mSOD1 mediated by RNA interference (RNAi). Here, we address this question using a longitudinal analysis to explore the neuroprotective effects induced by the treatment in *SOD1*^{G93A} mice. Our main objective is to elucidate how gene therapy changes the course of the disease during its early phase in *SOD1*^{G93A} mice, characterized by the degeneration of the most vulnerable population of fast-fatigable MN. Silencing of mSOD1 led to a significant protection of the motor function, improving mouse performance in specific behavioral tests for muscle strength and motor coordination. Treated mice displayed a partial protection of the vulnerable fast-fatigable MN in the lumbar spinal cord. However, AAV-mediated targeting of astrocytes for expression of miR SOD1 had most significant effects on the occupancy of the neuromuscular junctions (NMJ), which remained highly protected from ALS-induced denervation. In the *gastrocnemius* muscle, gene therapy induced a significant protection of the fast-twitch type IIB muscle fibers. Protection of the NMJ was also revealed by events of axonal sprouting and muscle fiber clustering. To further analyze the effects of treated astrocytes on spinal cord MN and identify potential gene candidates implicated in the therapeutic response, we performed a transcriptomic analysis of MN exposed to astrocytes expressing miR SOD1. Altogether, our results show that AAV-mediated gene therapy targeting mSOD1 in astrocytes has clear effects on spinal cord MN in *SOD1*^{G93A} mice by promoting functional innervation of the skeletal muscle.

2 | MATERIALS AND METHODS

2.1 | Animals and vector administration

All animal works were performed in accordance with the Swiss legislation and the European Community Council directive (86/609/EEC) for the care and use of laboratory animals. B6.Cg-Tg(SOD1*G93A) dl1Gur/J mice (The Jackson Laboratory, Bar Harbor, USA) were mated with C57BL/6J females (Charles River Laboratories, Bois des Oncins, France). Newborn pups were genotyped at birth by polymerase chain reaction (PCR) against human SOD1. ICV injections were performed on 2-days-old pups as previously described (Dirren et al., 2014). AAV vector suspensions were diluted in a physiologic solution of sodium chloride and mixed with 0.1% Fast Green FCF (Sigma-Aldrich) to visualize spread of the vector suspension throughout the ventricles. Three microliters of viral suspension were injected into the left lateral ventricle, using a 29G insulin syringe (B. Braun, Hessen, Germany).

2.2 | Viral vector production

The engineering and production of the AAV vectors were performed as previously described (Dirren et al., 2015). Briefly, the following microRNA sequences: miR SOD1: 5′-ATT ACT TTC CTT CTG CTC GAA-3′; miR SOD1-b: 5′-TAA AGT GAG GAC CTG CAC TGG-3′; and miR ctrl: 5′-AAA TGT ACT GCG CGT GGA GAC-3′ were introduced into the pre-microRNA backbone of murine miR-155′ and further cloned under the minimal GFAP promoter gfaABC$_1$D into the pAAV-MCS:gfp plasmid expression cassettes. The guide sequences miR SOD1 and miR SOD1-b were designed to specifically target the human SOD1 coding mRNA sequence (NM_000454) and did not recognize the murine SOD1 sequence (NM_011434).

For production of recombinant AAV9 particles, shuttle plasmids were co-transfected with the pDF9 helper plasmid into HEK293-AAV cells (Agilent Technologies, Santa Clara, USA). Cells were lysed 72 h following transfection. Viral particles were sequentially purified on iodixanol (Axis-shield, Dundee, United Kingdom) and ion-exchange affinity columns (GE Healthcare, Italy). Viral genomic copies were measured by TaqMan quantitative PCR (Invitrogen) using primers recognizing the human β-globin intron. The AAV9 vectors were injected at a titer of 1.4E14 viral genomes (VG)/mL for the behavioral study. For MN transcriptome analysis, a vector concentration of 2.9E14 VG/mL was used for ICV injection to achieve at least similar therapeutic efficacy.

2.3 | Behavioral testing and electromyography

Cohorts used for behavioral experiments were litter-matched. Evoked CMAP amplitude in the *triceps surae* was evaluated using the electromyographic apparatus (AD Instruments, Oxford, UK) as described previously (Dirren et al., 2015). For muscle strength measurements, each mouse was hold by the tail while lifting metal grids with defined weights of 20, 30, and 40 g. The maximal duration of the test was set at 30 s. Two successive trials were performed with each grid. The inter-trial interval was set at 30 s. For each grid, the score was calculated by multiplying the best time performance by the weight of the grid. For each mouse, the total score was defined as the sum of the scores obtained for each of the three grids. For the rotarod test, the mouse was placed on an accelerating rod, at a speed constantly increasing from 4 to 40 rpm, during a maximal period of 300 s. The performance was measured as the time during which the mouse was able to maintain itself on the rotating rod. For $SOD1^{G93A}$ mice, the end stage of the disease was defined as the time at which the animal could no longer right itself within 20 s after being placed on its flank.

2.4 | Histological analysis

Mice were sacrificed at the mentioned age or at end stage of the disease by intra-peritoneal injection of pentobarbital (Streuli Pharma, Uznach, Switzerland). Mice were transcardially perfused with PBS and one *gastrocnemius* muscle was directly embedded in Cryomatrix (Thermo Fisher Scientific), frozen on dry ice and kept at −80°C for muscle fiber analysis. Animals were further perfused with paraformaldehyde 4% (PFA, Karl Roth). The second *gastrocnemius* muscle and spinal cord were post-fixed in PFA 4% for 20 min and 90 min, respectively, before being transferred to a 25% sucrose solution.

Twenty-five μm thick sections of the lumbar spinal cord were cut on a cryostat and conserved free floating in PBS-azide solution. Twelve μm thick transversal sections of unfixed *triceps surae* muscle and 20 μm thick longitudinal sections of fixed *gastrocnemius* muscle were cut on a cryostat directly on glass slides.

For immunostaining, sections were incubated in a 0.15% Triton X-100, 2% bovine serum albumin, 3% normal horse serum blocking solution for 1 h at room temperature (RT). Sections were then incubated for 24 h at 4°C with primary antibodies diluted in blocking solution. Sections were washed and incubated with secondary antibody diluted in blocking solution for 1 h at RT.

Avidin–biotin/3,3′-diaminobenzidine method (Vectors Laboratories Inc. Burlingame, USA) was applied to reveal goat anti-ChAT (1:500, Chemicon Millipore, Billerica, USA), goat anti-MMP9 (1:1000, Sigma-Aldrich) and rabbit anti-IBA1 (1:2000, Wako Pure Chemical Industries, Osaka, Japan) immunostainings. Secondary antibodies were: biotinylated horse antigoat IgG or biotinylated goat antirabbit IgG (1:200, Vector BA). Forty-eight hours incubation of the primary antibody and nickel ammonium sulfate enhancement was used for MMP9 staining.

Other antibodies were: Rabbit anti-GFAP (DakoCytomation, Glostrup, Denmark), mouse anti-SV2 (1:40, Developmental Studies Hybridoma Bank [DSHB], University of Iowa, Iowa City, USA), and rabbit anti-NFM-145 (1:500, Chemicon Millipore), goat antirabbit Cy3, donkey antimouse Cy3, goat antirabbit alexa 488 (1:500, Jackson ImmunoResearch Laboratories, West Grove, USA) and tetramethylrhodamine α-bungarotoxin (1:500, Invitrogen). For muscle fiber type identification, transversal sections of *triceps surae* were stained with a cocktail of antibodies from DSHB: mouse anti-MyHC I (BA-D5, 1:500), mouse anti-MyHC IIa (SC-71, 1:500), mouse anti-MyHC IIb (BF-F3, 1:100), and rabbit antidystrophin (1:200, Abcam). The secondary antibodies used were: goat antimouse IgG2b-alexa 647 (1:500), goat antimouse IgG1-alexa 488 (1:500), goat antimouse IgM-AMCA (1:200) and goat antirabbit cy3 (1:500) (Jackson ImmunoResearch Laboratories).

2.5 | Quantification

For cell counts in the spinal cord, one every 10 sections were stained and counted. ChAT and MMP9-positive MN were manually counted in the ventral horn of the lumbar spinal cord section using an Olympus AX70 microscope (Olympus Corporation, Japan). Microglial activation was evaluated by manually counting Iba1-positive microglial cells. Astrocytic activation was assessed in the ventral horn of GFAP-stained lumbar sections. GFAP-positive total area was determined with ImageJ using percentile thresholding. For assessments of Iba1 and GFAP activation, five sections of the spinal cord representing 10 ventral horns per animal were used. Pictures were taken with a 20× objective on a Leica DM5500 microscope (Leica, Wetzlar, Germany).

Neuromuscular innervation was quantified on 20 μm-deep z-stack pictures of at least three fields of view per *gastrocnemius*. Sixty endplates identified using α-bungarotoxin staining were counted per muscle. Endplates were categorized as denervated, completely or partial innervated, according to the co-staining with the SV2 marker. Pictures were taken with a 20× objective on a Leica DM5500 microscope.

For muscle pattern analysis, pictures of the entire muscle section were taken with a 20× objective on an Olympus slide scanner VS120-L100. Pictures were post processed with a home-made Fiji macro and analyzed with MATLAB. For each channel, a minimal gray intensity threshold was set using sections stained with the secondary antibodies alone. For a given channel, values above the threshold were considered as positive and the muscle fiber type determined

accordingly. Muscle fibers with value below the threshold for all three channels were categorized as type IIx. Objects smaller than 150 μm^2 or bigger than 5000 μm^2 were excluded from the analyses.

Clustering analysis were done as follows: inter-fiber distances for fibers form the same subtype were determined according to their center of gravity. As each fiber is on average in contact with six other fibers, the median of the six shortest distances for each fiber was calculated. Median values were then averaged across all fibers from the same subtype. A second analysis was performed to determine the percentage of fibers in contact with another fiber from the same subtype. Briefly, the mean radius of a muscle fiber type was calculated based on the measured area of each fiber, and assuming that the fiber has a circular shape. If the distance between the centers of two fibers from the same subtype was longer than twice their radius plus two SD, the fibers were categorized as not in contact with each other.

2.6 | Laser-capture microdissection of spinal cord MN, RNA sequencing and analysis

Mice were sacrificed at 65 days by intra-peritoneal injection of pentobarbital (Streuli Pharma, Uznach, Switzerland). The lumbar part of the spinal cord with the vertebrae was directly embedded in OCT and frozen at −80°C. Fourteen μm thick sections were cut on a cryostat and stained with a 1% cresyl violet solution to reveal MN in lumbar spinal cord sections and guide laser-capture microdissection (PALM microscope, 20×, Zeiss). Total RNA was extracted from a pool of 500 MN per mouse with the microRNeasy kit according to manufacturer's instruction (Qiagen). RNA was quantified with a Qubit (fluorimeter from Life Technologies) and RNA integrity confirmed with a Bioanalyzer (Agilent Technologies). The SMARTer™ Ultra Low RNA kit from Clontech was used for reverse transcription and cDNA amplification according to manufacturer's instructions, starting with 5–6 ng of total RNA as input. The 200 pg of cDNA were used for library preparation using the Nextera XT kit from Illumina. Library molarity and quality was assessed with the Qubit and Tapestation using a DNA High sensitivity chip (Agilent Technologies). Pools of six libraries were loaded for clustering on Single-read Illumina Flow cells. Reads of 50 bases were generated on the Illumina HiSeq 2500 and 4000 sequencers. One sample was removed from the analysis because of the poor quality of the extracted RNA, another sample was removed because of low-sequencing depth and three other samples were removed because histological examination showed only low GFP expression levels.

The purity-filtered reads were adapters and quality trimmed with Cutadapt (v. 1.8, [Martin, 2011]). Reads matching to ribosomal RNA sequences were removed with fastq_screen (v. 0.9.3). Remaining reads were further filtered for low complexity with reaper (v. 15–065, [Davis et al., 2013]). Reads were aligned against *Mus musculus. GRCm38.86* genome using STAR (v. 2.5.2b, [Dobin et al., 2013]). The number of read counts per gene locus was summarized with htseq-count (v. 0.6.1, [Anders et al., 2015]) using *Mus musculus.GRCm38.86* gene annotation. Quality of the RNA-seq data alignment was assessed using RSeQC (v. 2.3.7, [Wang et al., 2012]). Reads were also aligned to the *Mus musculus.GRCm38.86* transcriptome using STAR (v. 2.5.2b, [Dobin et al., 2013]) and the estimation of the isoform abundance was computed using RSEM (v. 1.2.31, [Li & Dewey, 2011]).

Statistical analysis was performed in R (R version 3.4.0) on 18,371 protein coding genes with at least one read count in at least one sample. A multifactorial statistical model including the effects of (1) SOD1 silencing, (2) AAV transduction (GFP), and (3) Batch was used with DESeq2 to identify 95 miR SOD1 affected genes with a false discovery rate (FDR) ≤ 10% (Love et al., 2014). Prior to heatmap visualization, expression counts data were transformed with *regularized logarithm* (rlog), then batch-corrected. A gene ontology analysis for biological processes was performed with the software Gorilla (Eden et al., 2009), comparing the list of differentially expressed genes (FDR ≤20%) to the total list of identified genes. The set of RNA sequencing data is available through GEO with ID GSE148901.

2.7 | Quantitative PCR

cDNA from the SMARTer™ Ultra Low RNA kit from Clontech used for reverse transcription of the RNA obtained by laser micro-dissection were utilized to perform SYBR™ Green qPCR relative quantification. The primer pairs for specific genes were purchased from Qiagen (QuantiTect Primer Assay, listed in Table S1). Relative quantification was calculated after normalization to the reference genes X-prolyl aminopeptidase (Xpnpep1) and casein kinase 2 (Csnk2b).

2.8 | Statistical analysis

Data are presented as mean ± SEM or mean ± SD as stated in the figure legends. Statistical analyses were performed using either MATLAB or Prism 8 software and are specified in the figure legends. For electromyographic measurements (CMAP), as well as performance in the grid and rotarod tests, data were analyzed using a two-way (group x time) repeated-measures ANOVA followed by a Newman–Keuls post hoc test. The number of MN and NMJ were analyzed using one- and two-way ANOVA followed by Tukey's post hoc test for multiple comparisons. Analyses of muscle fiber clustering comparing wild type (WT) and treated mice was performed using two-tailed unpaired *t* test. The number and size of muscle fibers were analyzed using one-way ANOVA with Bonferroni post hoc test. For all statistical analyses, the α level of significance was set a 0.05.

3 | RESULTS

3.1 | Expression of miR SOD1 in astrocytes rescues neuromuscular function in *SOD1^{G93A}* mice

We assessed the effects of AAV-mediated miR SOD1 gene therapy on disease progression in *SOD1^{G93A}* mice. Mice were ICV injected at P2 with the AAV9-gfaABC$_1$D:GFP:miR SOD1 vector (AAV-miR SOD1) which drives expression of an artificial antihuman SOD1 miR in astrocytes (Dirren et al., 2015). As previously shown, AAV9 ICV injection in

neonatal mice leads to expression of GFP in the brain including the cerebral cortex, and along the spinal cord (Dirren et al., 2014). In the injected mice, GFP was expressed in astrocytes in the lumbar spinal cord, at day 65 and end stage (day 153–185) (Supplemental Figure S1). To assess neuroprotective effects of the astrocyte-specific silencing of SOD1, the treated mice were compared to *SOD1*^{G93A} mice injected with a similar vector encoding a scramble miR sequence (AAV-miR ctrl), noninjected *SOD1*^{G93A} mice (untreated), and WT littermates. Neuromuscular function was assessed along the course of the disease using electromyography and behavioral tests (Figure 1a). Amplitude of the muscle evoked response (CMAP) was measured every week in the *triceps surae* (Figure 1b). The effects of the treatment were consistent with the results reported by (Dirren et al., 2015). Until day 73, there were no significant effects of AAV-miR SOD1, as CMAP values declined to 62 ± 4.3 mV in the treated mice, a value only slightly higher than in both control groups of *SOD1*^{G93A} mice. CMAP amplitude then increased in the AAV-miR SOD1 group, to reach 88 ± 7.3 mV at day 87, and then stayed stable until day 136. In contrast, CMAP values further decreased in the AAV-miR ctrl and untreated mice. Another miR SOD1-b sequence also targeting human SOD1 showed similar effects, which are therefore not specific to the miR sequence (Supplemental Figure S2). Muscle strength and motor coordination were evaluated with the grid and rotarod tests, respectively (Figure 1c, d). Control *SOD1*^{G93A} mice showed a progressive loss of muscle strength detectable from day 93 on (Figure 1c). As compared to control groups, AAV-miR SOD1 significantly improved muscle strength from day 119 until end stage (Figure 1c). In the rotarod test, the latency to fall was only marginally prolonged in the AAV-miR SOD1 treated mice, when compared to untreated *SOD1*^{G93A} mice, reaching significance only at later stages of the disease (Figure 1d). These results indicate that silencing of mSOD1 in astrocytes protects from the loss of

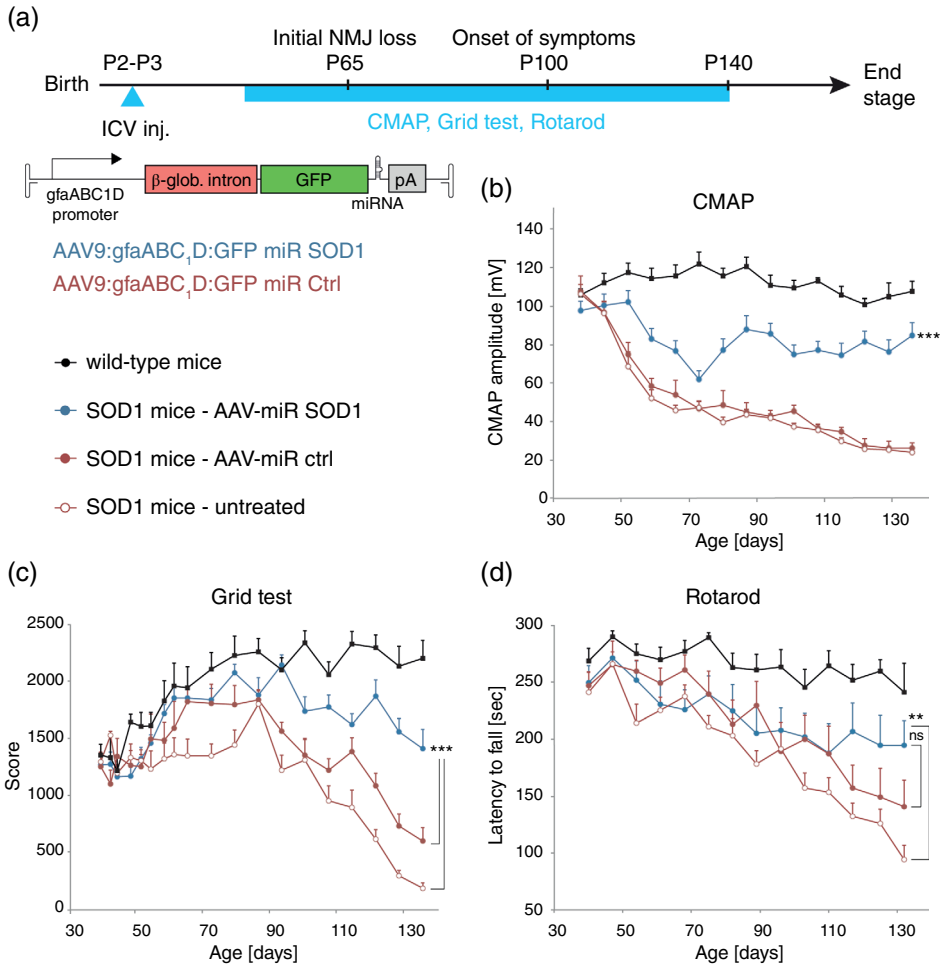

FIGURE 1 AAV-miR SOD1 targeting of astrocytes preserves neuromuscular function. Neuromuscular function is assessed by electromyography and behavioral testing. (a) Schema of the longitudinal experiment indicating the analysis time points. (b) Amplitude of the evoked compound muscle action potential (CMAP) recorded in the *triceps surae*. Note the rapid decrease of CMAP amplitude in the untreated and AAV-miR ctrl injected *SOD1*^{G93A} mice between day 45 and 66. There is a progressive rescue of CMAP values in the AAV-miR SOD1 treated group, from day 73 onwards. (c) The grid test is used to evaluate the strength of the four limbs. Note the marked decrease of the score in the untreated and AAV-miR ctrl injected *SOD1*^{G93A} mice, from day 86 on. A significant rescue of muscle strength is observed in the AAV-miR SOD1-treated mice. Statistical analysis for b and c: two-way ANOVA (group x time) repeated measures with Bonferroni post hoc test; ***$p < .001$. (d) Motor coordination is measured in the Rotarod test. Note the progressive loss of performance in ALS mice, starting at day 75. AAV-miR SOD1 induces a late improvement of the motor coordination, from day 117 on. Statistical analysis: one-way ANOVA with Newman–Keuls post hoc test; *$p < .05$, **$p < .01$. Data represent mean ± SEM. $n = 12$ mice per group

the neuromuscular function in *SOD1*^{G93A} mice, mainly improving muscle strength as compared to untreated mice.

3.2 | Expression of miR SOD1 in astrocytes protects MN in the lumbar spinal cord but has no effect on the inflammatory response

Next, we analyzed spinal cord tissue at various time points over the disease process, from day 65 (initial drop of the CMAP amplitude) until end stage. The number of choline acetyltransferase (ChAT)-positive MN was determined in the lumbar region of the spinal cord (Figure 2a, b). At day 65, MN loss was only marginal in *SOD1*^{G93A} mice compared to WT mice (Figure 2b). However, the number of ChAT-positive MN was significantly decreased in all groups at day 140. At end stage, the number of surviving MN reached 10.1 ± 2.1 and 12.2 ± 2 MN (mean ± SEM) per section in the AAV-miR ctrl injected and control untreated ALS mice, respectively. In the AAV-miR SOD1 treated mice however, the number of ChAT-positive MN was significantly increased (14.7 ± 2.1 MN per section) (Figure 2b), similar to the effects reported in (Dirren et al., 2015).

To assess if AAV-miR SOD1 could prevent astrocytic and microglial activation in the spinal cord, we measured the area of GFAP immunoreactivity and the number of Iba1-positive microglial cells on

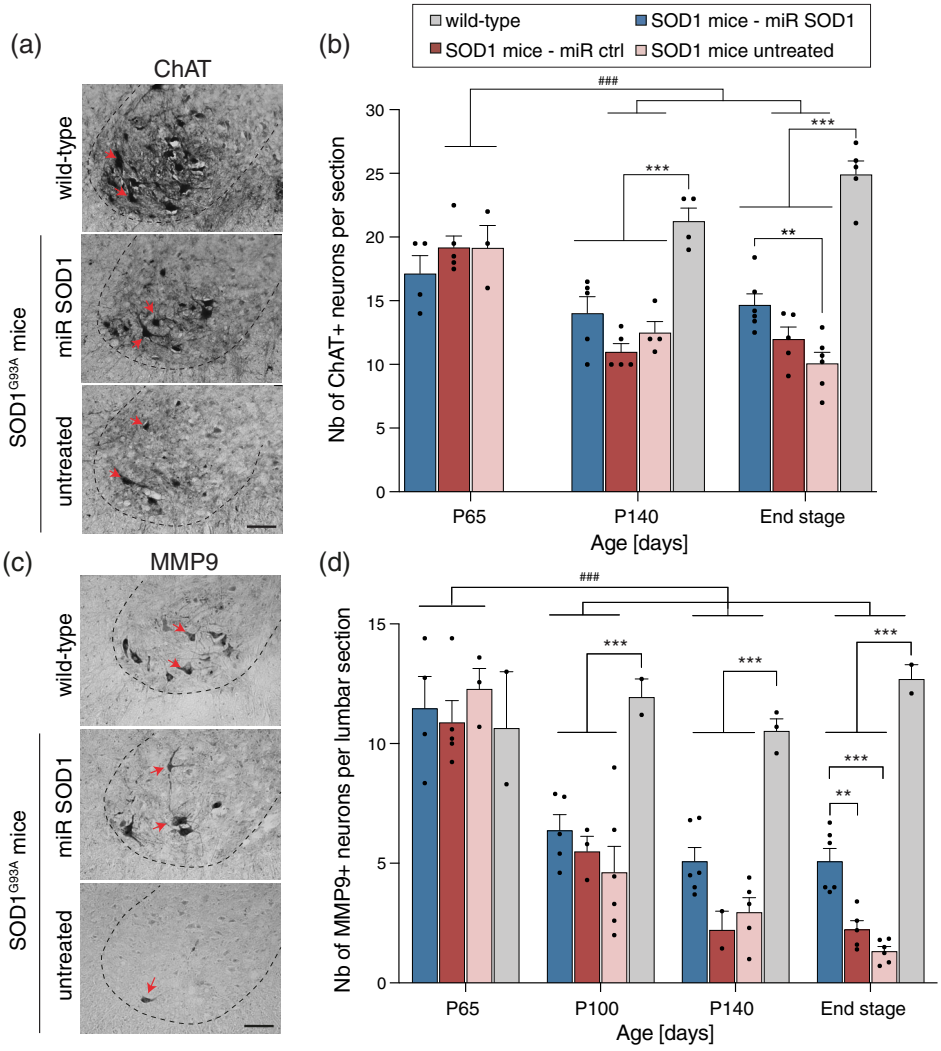

FIGURE 2 AAV-miR SOD1 targeting of astrocytes has protective effects on fast-fatigable motoneurons in the lumbar spinal cord. (a) Representative pictures of ChAT+ MN (red arrows) in the lumbar spinal cord at end stage. (b) Quantification of the number of ChAT+ MN per section of the lumbar spinal cord, from 65 days of age until end stage. Statistical analysis: two-way ANOVA (time effect) with Tukey's post hoc test; compared to day 65, there is a significant loss of ChAT+ MN in the AAV-miR ctrl and untreated *SOD1*^{G93A} mice only ($^{###}p < .001$). One-way ANOVA at individual time points with Tukey's post hoc test; $^{**}p < .01$, $^{***}p < .001$. At end stage, the number of MN is significantly higher in the AAV-miR SOD1 group compared to untreated *SOD1*^{G93A} mice. (c) Representative pictures of fast-fatigable MN highly immunoreactive for MMP9 (white arrows) at end stage. (d) Average number of fast-fatigable MN per section identified by high MMP9 immunoreactivity. Statistical analysis: two-way ANOVA (time effect) with Tukey's post hoc test; compared to day 65, there is a significant loss of MMP9+ MN in all groups of *SOD1*^{G93A} mice ($^{###}p < .001$). One-way ANOVA at individual time points with Tukey's post hoc test; $^{**}p < .01$, $^{***}p < .001$. There is a significant loss of MMP9+ MN per section in *SOD1*^{G93A} mice from day 100 on. Note the significant protection of MMP9+ MN in the AAV-miR SOD1 treated mice at end stage. Data represent mean ± SEM. Scale bars: 50 μm

lumbar sections at day 65, 100 and 140 (Supplemental Figure S3a–d). As expected, a significant astrocytic and microglial activation was observed in *SOD1*^{G93A} mice, from day 100 onwards. However, there were no significant differences in the group treated with AAV-miR SOD1 as compared to control ALS mice. These results indicate that the treatment did not have any major effects on the progression of astrogliosis and microgliosis in *SOD1*^{G93A} mice.

3.3 | AAV-miR SOD1 injection protects a subpopulation of MMP9 expressing MN

Since all MN subtypes are not equally affected in ALS mice, we further evaluated the effects of the treatment based on the expression of MMP9, a marker highly expressed in fast-fatigable MN, which display highest vulnerability to mSOD1-induced toxicity (Figure 2c) (Kaplan et al., 2014; Pun et al., 2006). At day 65, the number of lumbar MN highly positive for MMP9 was still very similar to WT mice in all groups of *SOD1*^{G93A} mice (Figure 2d). At day 100 however, the loss of fast-fatigable MN already reached 50% and further declined until end stage, at which time point only 1.5 ± 0.5 and 2.2 ± 0.8 fast-fatigable MN were found per lumbar section in the untreated and AAV-miR ctrl injected mice, respectively. In the AAV-miR SOD1 treated mice, the number of MMP9-positive MN remained stable from day 100 onwards. At end stage, we measured 5.1 ± 1.3 MN per lumbar section (mean ± SEM), a number significantly higher than in control groups of *SOD1*^{G93A} mice (Figure 2d). These results show that silencing mSOD1 in astrocytes rescues a subpopulation of fast-fatigable MN with high MMP9 immunoreactivity.

3.4 | Expression of miR SOD1 in astrocytes rescues NMJ

Despite the partial rescue of spinal cord MN, AAV-miR SOD1 injection preserved CMAP values (see Figure 1b), which indicates that the treatment may have additional protective effects at the level of the NMJ. To address this possibility, we analyzed NMJ occupancy in the *gastrocnemius* muscle at day 65, 100, 140, and end stage. Acetylcholine receptors were stained with alpha-bungarotoxin to reveal motor endplates, and colocalization with the antisynaptic vesicle protein 2 (SV2) marker was used to quantify NMJ occupancy (Figure 3a). Complete overlap between the α-bungarotoxin and SV2 staining accounted for the presence of a fully innervated NMJ (Figure 3a, b). At day 65, all groups of *SOD1*^{G93A} mice, including the group treated with AAV-miR SOD1, displayed a significant loss of fully innervated NMJ as compared to WT mice (AAV-miR SOD1: 61 ± 7% occupancy; WT: 94 ± 2%, mean ± SEM) (Figure 3b). The innervation of motor endplates further declined until end stage in ALS mice either untreated (13 ± 7%) or injected with AAV-miR ctrl (16 ± 5%). In the AAV-miR SOD1 treated group however, the proportion of fully innervated NMJ increased to 84 ± 5% by 100 days, and remained significantly rescued until end stage (73 ± 7%), only marginally decreased in comparison to WT mice (94 ± 32%) (Figure 3b). Therefore, injection of the AAV-miR SOD1 vector targeting astrocytes has strong neuroprotective effects on NMJ occupancy, consistent with the results shown in (Dirren et al., 2015).

3.5 | Expression of miR SOD1 in astrocytes protects mainly fast-twitch type IIB muscle fibers from atrophy

To further assess the rescue of motor units by AAV-miR SOD1 injection, we analyzed the morphology and composition of the *triceps surae* at end stage. In particular, changes in the number, size and type of muscle fibers were assessed by immunohistochemistry in the *gastrocnemius* and *plantaris* muscles at end stage. In mice, fast-twitch glycolytic type IIB muscle fibers are innervated by fast-fatigable MN, fast-twitch oxidative type IIA fibers by fatigue-resistant MN, and slow-twitch oxidative type I fibers by slow MN. Some fibers display a phenotype which is intermediate between type IIA and IIB, defined as type IIX. Major fiber types were identified using specific staining for myosin heavy chain (MyHC) isoforms (Figure 4a). Dystrophin staining was used to delineate fiber circumference and quantify the number and mean area of individual muscle fibers (Figure 4b). As expected, there was a marked muscle atrophy in *SOD1*^{G93A} mice either untreated or injected with the AAV-miR ctrl vector. Atrophy was most evident in the *gastrocnemius* muscle, characterized by a major loss of type IIB muscle fibers, but was less pronounced in the *plantaris* (mixed fiber types) and *soleus* (type I and IIA) muscles (Figure 4a). Compared to WT mice, the total number of fibers in the *gastrocnemius* muscle was decreased by more than 50% in control *SOD1*^{G93A} mice (Figure 4c). In contrast, there was a clear protection of muscle fibers in the AAV-miR SOD1 treated mice. Both the number and the area of the type IIB fibers remained nearly unchanged in the AAV-miR SOD1 treated mice as compared to WT animals, whereas these parameters were dramatically decreased in the control groups (Figure 4d, e). In contrast, there was no significant difference neither in the number, nor in the area of type IIA, type I and type IIX fibers across groups (Figure 4d, e). Overall, these results indicate that AAV-miR SOD1 treatment has major protective effects against atrophy of type IIB muscle fibers, consistent with the observed protection of the fast-twitch fatigable MN in the lumbar spinal cord (Figure 2d).

3.6 | miR SOD1 gene therapy targeted to astrocytes induces axonal sprouting and muscle fiber type grouping

The significant rescue of NMJ occupancy observed in the AAV-miR SOD1-treated group indicates that motor nerve sprouting may have occurred in the *gastrocnemius* muscle. To qualitatively assess axon sprouting events, we performed a co-staining of NMJ with α-bungarotoxin, SV2 and NFM-145, a marker for axonal neurofilaments. At day 100, terminal sprouting characterized by the

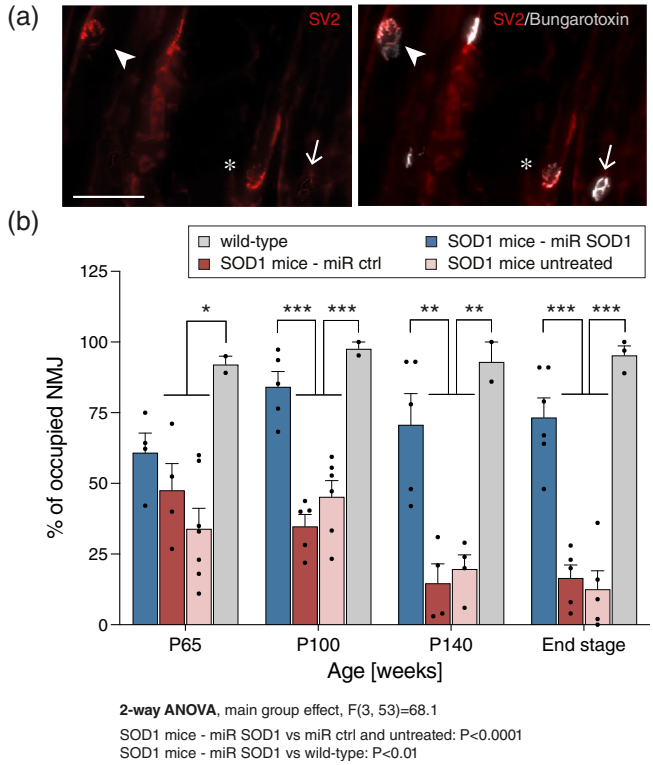

FIGURE 3 The occupancy of the neuromuscular junctions is rescued in the *gastrocnemius* muscle of *SOD1*^{G93A} mice treated with AAV-miR SOD1. Analysis of the innervation of motor endplates in the *gastrocnemius* muscle. (a) Immunostaining for SV2 (synaptic marker) and α-bungarotoxin labeling of the motor endplate showing a fully innervated NMJ (*, markers are fully colocalized), a partially innervated NMJ (arrowhead) and an unoccupied motor endplate (arrow). (b) Quantification of the percentage of fully innervated NMJ in the *gastrocnemius* muscle. At day 65, NMJ occupancy is significantly decreased in all groups of *SOD1*^{G93A} mice. Note the significant rescue of NMJ occupancy at days 100, 140 and end stage in the *gastrocnemius* muscle of AAV-miR SOD1-treated *SOD1*^{G93A} mice, as compared to the continuous decrease observed in the AAV-miR ctrl-injected and untreated mice. Statistical analysis: two-way ANOVA (main group effect) with Tukey's post hoc test. One-way ANOVA at individual time points with Tukey's post hoc test; *p < .05, **p < .01, ***p < .001. Data represent mean ± SEM. Scale bar 75 μm

presence of axons extending beyond the motor endplate was indeed observed in AAV-miR treated mice (Figure 5a), which indicates that the treatment may have induced reinnervation of vacant endplates.

In neurogenic muscle atrophy, muscle fiber type grouping is often observed when denervation is followed by reinnervation. To assess plastic changes in the skeletal muscle, we sought to determine the level of clustering of muscle fibers by comparing WT and AAV-miR SOD1-treated ALS mice. This analysis was only possible on non-atrophied muscle tissues. While the overall number of muscle fibers was similar in both groups (see Figure 4c), MyHC staining revealed signs of fiber-type grouping in the treated *SOD1*^{G93A} mice. In Figure 5b, this effect is particularly evident in the *plantaris* muscle, where different types of muscle fibers are intermingled. To quantify the clustering of type I, IIA and IIX muscle fibers, we measured the average distance between fibers from the same type (Figure 5c) and the percentage of fibers that are adjacent to at least one other fiber from the same subtype (Figure 5d). Both parameters revealed significant fiber grouping effects for all three fiber types in the *gastrocnemius* and *plantaris* muscles of AAV-miR SOD1-treated mice. As there is no loss of type IIB fibers to explain this apparent clustering in the AAV-miR SOD1-treated mice, it is likely to reflect fiber type conversion due to reinnervation of vacant endplates via the outgrowth of motor axon collaterals.

3.7 | Transcriptional signature of MN in the spinal cord of miR SOD1-treated ALS mice reveals changes in genes controlling microtubule stability

Next, we sought to explore the changes in gene expression induced by the presence of mSOD1-expressing astrocytes in the lumbar spinal cord. Similar to our previous experiment, *SOD1*^{G93A} mice were ICV injected at 2 days of age either with the AAV-miR SOD1 vector or with AAV-miR ctrl. An additional group of noninjected *SOD1*^{G93A} littermate mice was included in the experiment. At day 65, a transcriptomic analysis was performed on MN captured by laser microdissection in the ventral horn. This time point was selected for analysis of gene expression across conditions, as the number of surviving MN was previously found to be very similar in each group (see Figure 2b), avoiding any confounding effects due to differences in MN survival. Whole transcriptome was analyzed by next generation sequencing, reaching on average 5.3E7 ± 1.0E7 reads per sample (mean ± SD), out of which 4.2E7 ± 0.9E7 reads where aligned to the reference mouse genome.

With the statistical tool DESeq2, we found 95 genes with changes in expression induced by SOD1 silencing with a false discovery rate (FDR) below 10% (Figure 6a and Supplemental Table S2). Sixty-four genes were significantly upregulated and 31 genes downregulated in the AAV-miR SOD1 mice, as compared to untreated and AAV-miR ctrl injected *SOD1*^{G93A} mice. For several differentially expressed genes, the changes in gene expression were confirmed by qPCR (Supplemental Table S1). A gene ontology analysis for biological processes was performed with the software Gorilla (Eden et al., 2009), taking into account the genes with a FDR below 20% (473 genes) as compared to the total list of identified genes. Analysis showed a significant enrichment for genes involved in heme biosynthesis (p = 8.15E-9), chromatin organization (p = 8.53E-5), microtubule stability (p = 5.24E-4) and synaptic glutamatergic transmission (p = 7.49E-4). To assess the presence of transcripts derived from astrocytic or microglial material contaminating the microdissected MN, the level of three astrocytic markers (*Gfap*, *Aldh1l1*, *S100b*) and three microglial markers (*Aif1*, *Tmem119*, *Trem2*) was compared to MN markers (*Chat*, *Slc18a3*, *Mmp9*). There was no difference between groups in the level of astrocytic markers (Supplemental Figure S4a), indicating that the amount of contaminating astrocyte-derived material was very similar across conditions. However, we found an upregulation of microglial transcripts in the AAV-miR SOD1 treated

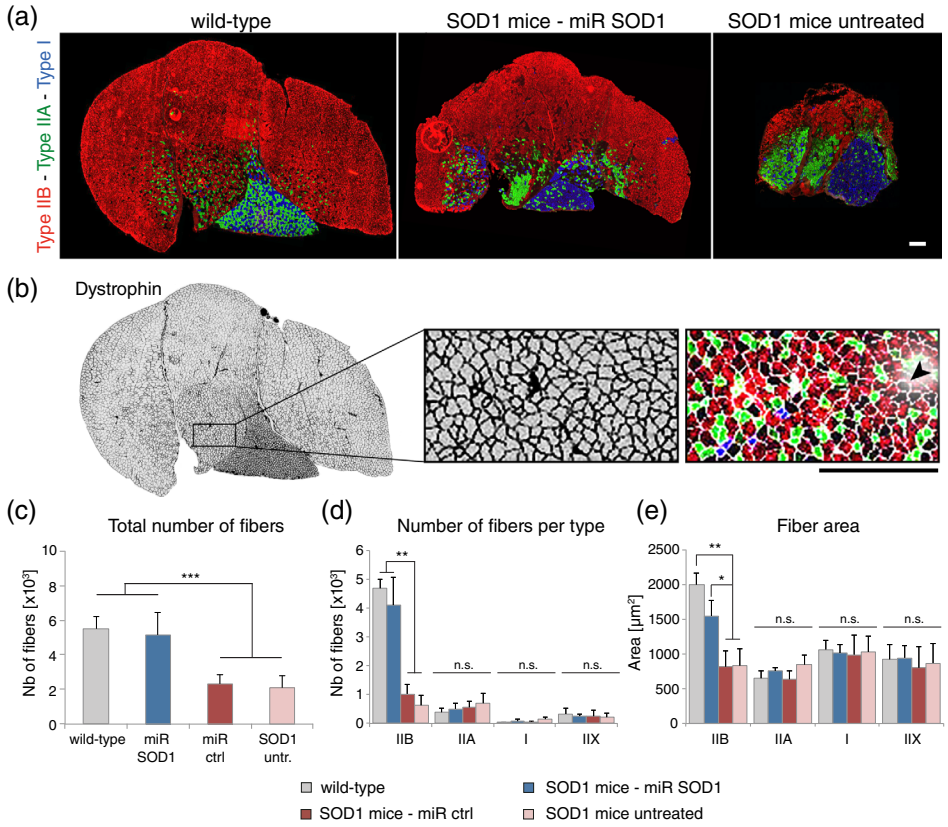

FIGURE 4 AAV miR SOD1 treatment protects against the loss of type IIB muscle fibers. (a) Representative images of transversal sections of the *triceps surae* muscle in WT, AAV-miR SOD1 treated and untreated ALS mice at end stage. Sections were co-immunostained for three MyHC isoforms: isoform IIb (red) shows type IIB fibers forming fast-twitch fast-fatigable motor units; isoform IIa (green) shows type IIA fibers forming fast-twitch fatigue-resistant motor units; isoform I (green) shows type I fibers forming slow-twitch motor units. Note the lack of muscle atrophy in the *SOD1*^{G93A} mice treated with AAV-miR SOD1, as compared to untreated ALS mice. Scale bar: 300 µm. (b) Dystrophin staining (left panel) delineates individual muscle fibers, the type of which is determined according to co-immunostaining for MyHC isoform (right panel). Fibers negative for all three MyHC isoforms are defined as type IIX (arrowhead). Scale bar: 300 µm. (c) Quantitative analysis of the total number of fibers in the *gastrocnemius* and *plantaris* muscles at end stage. Note the significant protection against muscle fiber loss in the *SOD1*^{G93A} mice treated with AAV-miR SOD1. (d) Number of muscle fibers for each fiber type. (e) Mean area of individual muscle fibers, according to fiber type. Note the significant protection of the number and size of type IIB muscle fibers in AAV-miR SOD1 treated *SOD1*^{G93A} mice. Data represent mean ± SD; $n = 5$ for all conditions, except WT mice ($n = 4$). Statistical analysis: one-way ANOVA with Bonferroni post hoc test; n.s. not significant, $^{*}p < .05$, $^{**}p < .01$, $^{***}p < .001$

mice as compared to the control groups (Supplemental Figure S4b). This effect was mainly due to the higher level of *Trem2* expression in this condition (FDR = 0.16, $p = .005$), which might be related to the observed neuroprotective effects of the treatment.

Next, we sought for gene expression changes related to possible effects of AAV-miR SOD1 on neuronal plasticity. As compared to control conditions, we found three genes of the Stathmin family to be downregulated (*Stmn2*, *Stmn3*, and *Stmn4*) (Figure 6b). Stathmins are involved in neuronal plasticity and have been shown to destabilize microtubules and inhibit their polymerization by sequestering αβ-tubulin heterodimers (Chauvin & Sobel, 2015). The *Mapt* gene encoding the microtubule-binding protein tau was also downregulated in the AAV-miR SOD1 condition (Figure 6b). In addition, expression of the α-tubulin-acetyl transferase gene *Atac1* was significantly downregulated, in contrast to the expression of the kinesin motor proteins Kif18a and Kif18b, which were upregulated following SOD1 silencing (Figure 6b). Overall, these changes in gene expression showed that the AAV-miR SOD1 treatment affects microtubule dynamics in spinal cord MN, at the level of factors controlling the polymerization, stability and post-translational modifications of tubulin. Furthermore, the expression of *Fbxo5* was significantly upregulated in the treated mice (Figure 6b). *Fbxo5* is a suppressor of Cdh1 implicated in axoneogenesis in the adult CNS (Haenold et al., 2014). Unexpectedly, AAV-miR SOD1 treated mice showed downregulation of BDNF (Figure 6b), a neurotrophic factor implicated in the competition between axons for making neuromuscular connections (Je et al., 2013). Importantly, the effects of BDNF depend on the proteolytic conversion from the pro- to the mature form of the neurotrophic factor. Indeed, the transcription of *Furin*, a key enzyme in this process, was increased in AAV-miR SOD1-injected mice (Figure 6b).

Changes in MN activity were previously observed in models of SOD1-related ALS, shifting from hyper- to hypoexcitability in adult spinal MN (Delestrée et al., 2014; Martínez-Silva et al., 2018). In addition, expression of mSOD1 affects the ability of astrocytes to regulate glutamate receptor expression in MN (Damme et al., 2007). Here, AAV-miR SOD1 had a significant effect on the expression of several

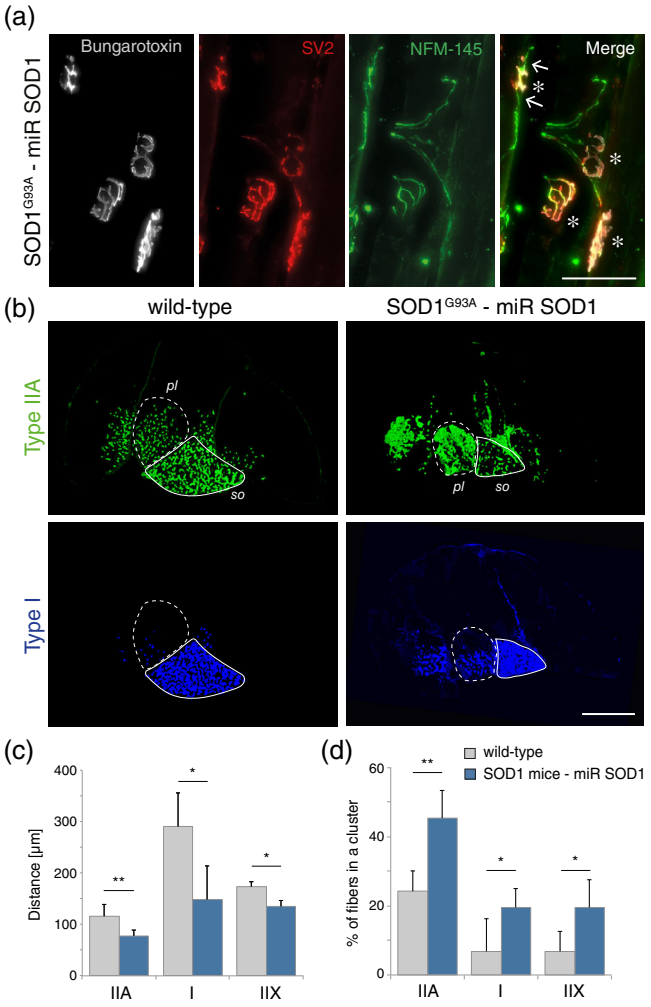

FIGURE 5 Axonal sprouting and fiber type grouping in the *triceps surae* of AAV-miR SOD1-treated *SOD1*^{G93A} mice. (a) Representative photomicrograph of NMJ stained with α-bungarotoxin (white), SV2 (red) and NFM-145 (green) in the *gastrocnemius* muscle of an AAV-miR SOD1 treated *SOD1*^{G93A} mouse at day 100. The co-localization of SV2 and α-bungarotoxin indicates complete endplate innervation in all NMJ (*). The arrows show a NFM-145-positive axon extending beyond the motor endplate, which is considered as a terminal sprouting event. Scale bar: 75 µm. (b) Transversal sections of the *triceps surae* muscle stained for type IIa and type I MyHC to reveal the distribution of muscle fiber types in a WT and an AAV-miR SOD1-treated *SOD1*^{G93A} mouse. Note the grouping of type IIA and type I muscle fibers in the treated ALS mouse (right panels), particularly evident in the *plantaris* (*pl*, dotted line) and *soleus* (*so*, solid line) muscles. Scale bar: 1 mm. (c) Quantification of the average minimal distance between fibers from the same type. A reduced distance is indicative of fiber type grouping. (d) Quantification of the percentage of fibers in direct contact with another fiber from the same type. Note that for both parameters, there is a significant increase of the clustering for all the fiber types analyzed in the AAV-miR SOD1 treated *SOD1*^{G93A} mice. Data represent mean ± SD; $n = 4$ WT mice and $n = 5$ AAV-miR SOD1-treated *SOD1*^{G93A} mice. Statistical analysis: two-tailed unpaired Student's *t* test; $^{*}p < .05$, $^{**}p < .01$

genes involved in synaptic neurotransmission. Notably, subunit-encoding genes of the ionotropic glutamate receptor family such as *Gria1* (glutamate ionotropic receptor 1, AMPA1) and *Grid2* (glutamate ionotropic receptor delta type subunit 2) were significantly down-regulated (Supplemental Figure S5a, b). Similarly, the levels of the transcripts encoding the gamma-aminobutyric acid (GABA) A receptor subunits γ1 and γ2 were significantly reduced in the AAV-miR SOD1 treated condition (Supplemental Figure S5c, d). Genes implicated in cholinergic neurotransmission such as *ChAT* (choline acetyl transferase) and *Slc5a7* (high affinity choline transporter 1) were also down-regulated (Supplemental Figure S5e, f). Changes in the expression of genes implicated in neurotransmission may reflect MN plasticity and motor circuit homeostasis following AAV-miR SOD1 gene therapy targeting astrocytes.

4 | DISCUSSION

In the *SOD1*^{G93A} mouse model of ALS, we show that gene therapy to express specifically in astrocytes an artificial miR driving the selective silencing of human SOD1 leads to an improvement of the neuromuscular function in *SOD1*^{G93A} ALS mice. In the hind limbs, the effects of the treatment are characterized by the protection of fast-fatigable motor units. The use of an AAV9 vector combined with the gfaABC$_1$D promoter leads to transgene expression mainly in astrocytes until disease end stage. Of note, expression of the transgenes in other cell types including some neuronal cells cannot be ruled out (Griffin et al., 2019; Taschenberger et al., 2017), especially in disease conditions which can strongly affect cell transcriptional activity (Hol et al., 2003). Furthermore, miRNAs can be transferred from astrocytes to other cell types, including neurons (Gharbi et al., 2020), which could also extend the effects of gene therapy beyond the glial cells primarily targeted by the vector. Nevertheless, these results support the important role of astrocytes in ALS and this cell type should be considered as a prime target for gene therapy. Along these lines, WT glial-restricted progenitor cells implanted into the spinal cord of *SOD1*^{G93A} rats were shown to efficiently differentiate into astrocytes and improve neuromuscular function (Lepore et al., 2008). Similar results were obtained by transplanting astrocytes derived from healthy human iPSC into the spinal cord of *SOD1*^{G93A} mice (Kondo et al., 2014). Conversely, the transplantation of astrocytes expressing mSOD1 in WT mice leads to MN dysfunction, with negative effects on the neuromuscular function (Papadeas et al., 2011).

Although AAV-miR SOD1 gene therapy targeting astrocytes does not reduce astrogliosis, it appears to enhance the propensity of MN to form new synapses on motor end plates. Astrocytes are known to release molecules that modulate synaptic activity and also control the formation, stabilization and elimination of synapses (reviewed in [Clarke & Barres, 2013]). Astrocytes can secrete matricellular proteins such as thrombospondin (TSB), secreted protein acidic and rich in

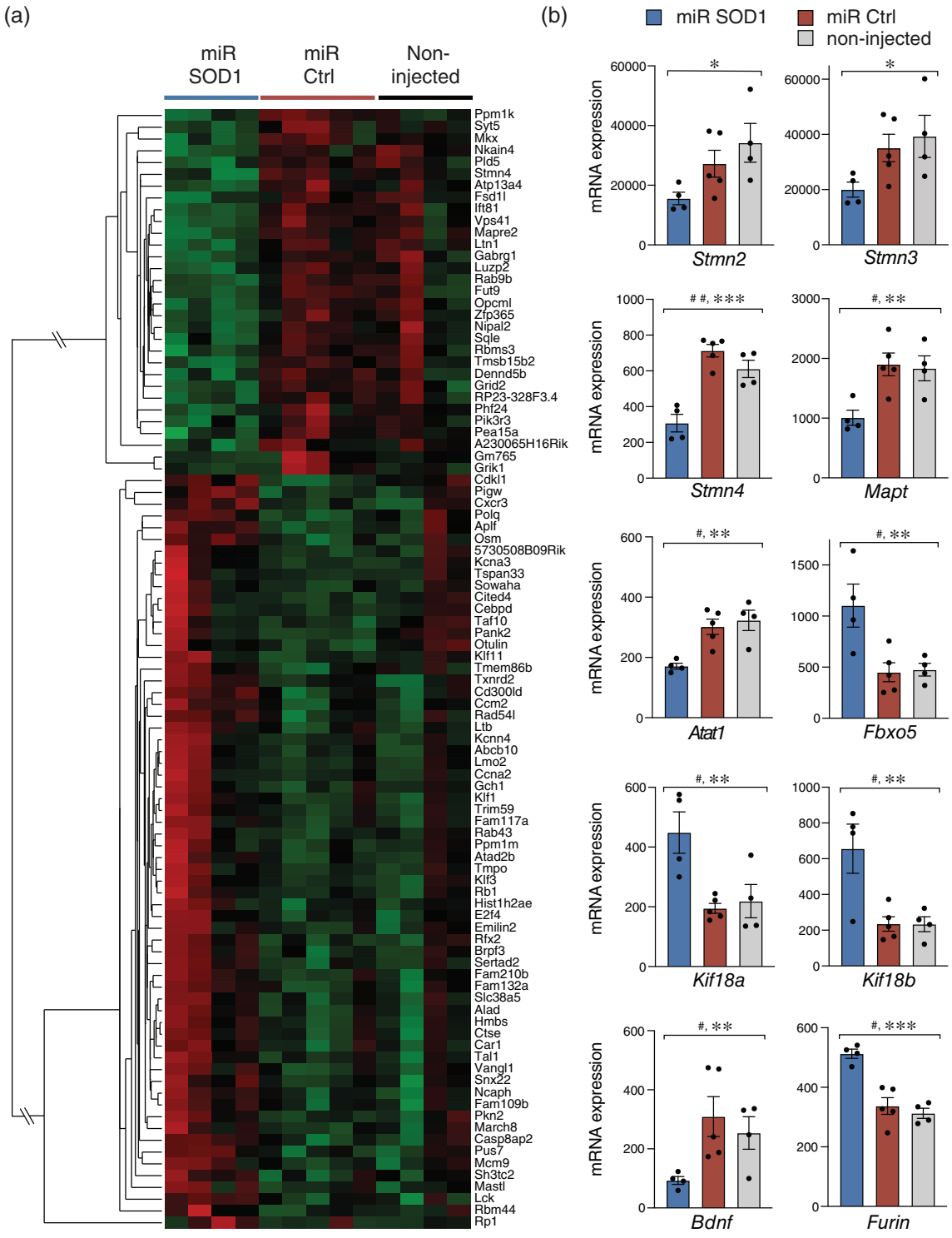

FIGURE 6 Differentially expressed genes in spinal cord motoneurons of *SOD1*^{G93A} mice following AAV-miR SOD1 targeting of astrocytes. A multifactorial statistical model with DESeq2 is used to identify 95 genes differentially expressed in MN of AAV-miR SOD1 treated *SOD1*^{G93A} mice ($n = 4$) as compared to AAV-miR ctrl ($n = 5$) and noninjected *SOD1*^{G93A} mice ($n = 4$). (a) Genes with expression changes at a false discovery rate (FDR) ≤ 10% are shown in the hierarchical clustering dendrogram. (b) Histogram plots showing differences in mRNA expression for individual genes either regulating microtubule stability or related to MN plasticity. Data represent mean ± SEM. Statistical analysis: FDR adjusted *P* value: # *P*adj < 0.1, ## *P*adj < 0.2; one-way ANOVA: $^{*}p < .05$, $^{**}p < .01$, $^{***}p < .001$

cysteine like1 (SPARCL1), and SPARC (an antagonist of SPARCL1 also known as osteonectin), which have been shown to regulate synaptogenesis (Blakely et al., 2015; Christopherson et al., 2005; Kucukdereli et al., 2011). These mechanisms are typically mediated by astrocytes in close contact with synaptic connections. However, it is unclear how the astrocyte-MN crosstalk in the spinal cord may

regulate the distal formation of NMJ. Factors secreted by astrocytes and Schwann cells can mediate synapse formation in spinal MN cultures (Ullian et al., 2004). In *Drosophila*, glial cells present at the NMJ contribute to the remodeling of the synaptic connections by removing presynaptic debris and immature boutons (Fuentes-Medel et al., 2009). In vertebrates, it is mainly terminal Schwann cells which have been reported to control the formation, maintenance, repair and pruning of the synapse at the NMJ (Feng & Ko, 2008). In $SOD1^{G93A}$ mice, Schwann cells express Sema3a, a chemorepellent inhibiting axonal outgrowth at the NMJ of type IIB/IIX muscle fibers (Winter et al., 2006). Furthermore, the loss of terminal Schwann cells as well as macrophage infiltration are observed specifically at type IIB fibers after induced partial denervation in ALS mice (Harrison & Rafuse, 2020). These findings are likely to underlie the deficits in sprouting of type IIB fibers in ALS (Frey et al., 2000; Gordon et al., 2010; Schaefer et al., 2005).

AAV-miR SOD1 treatment enhances limb strength in the grip test, which is coherent with the observed protection of type IIB muscle fibers in the *triceps surae*, and the significant protection of MN with high MMP9 expression. These neurons may constitute a pool of fast-fatigable MN protected from neurodegeneration. This effect might as well reflect a gain of MMP9 expression in the remaining pool of MN, similar to what has been observed in another transgenic mouse model of ALS following suppression of the cytosolic TDP-43 transgene (Spiller et al., 2016). It remains however unclear whether the expression of MMP9 is necessary for NMJ reinnervation. In non-diseased conditions, NMJ reinnervation following injury has been found to occur more rapidly in fast-fatigable than in slow MN (Nishizawa et al., 2006). In rodent models of ALS however, sprouting events appear to mainly occur in fatigue-resistant and slow MN, whereas there is so far no evidence for similar effects in the fast-fatigable pool (Frey et al., 2000; Harrison & Rafuse, 2020; Schaefer et al., 2005). Here, the remarkable protection of type IIB fibers indicates that gene therapy targeting astrocytes in the $SOD1^{G93A}$ mouse model of ALS may enhance reinnervation even in fast muscles.

Fiber type grouping is observed in patients suffering from spinal and bulbar muscular atrophy, but to a lesser extent in ALS patients (Baloh et al., 2007; Jokela et al., 2016). In contrast to other neuromuscular disorders, it is therefore possible that either the ability of MN to remodel neuromuscular synaptic connections is impaired in ALS, or that disease causes extensive degeneration before muscle fiber grouping can be observed. The increase in clustering of type I and type IIA muscle fibers shows that the AAV-miR SOD1 treatment enhances the ability of the surviving MN to make new functional connections with the muscle towards disease end stage, and that this effect is likely to involve all types of MN in the spinal cord. Similarly, treatment of $SOD1^{G93A}$ ALS mice with antisense oligonucleotides (ASO) targeting SOD1 also induces a gain in CMAP amplitude at a later stage of the disease, indicating possible rescue effects also with this mode of treatment (McCampbell et al., 2018). However, it is unclear to which extent the ASO treatment targets mSOD1 expression in astrocytes.

The analysis of gene pathways in MN highlights changes in the expression of genes regulating microtubule dynamics following AAV-miR SOD1 treatment. In particular, genes of the Stathmin family are consistently downregulated, which may reflect increased microtubule stability. Previous studies have shown in a mouse model of spinal muscular atrophy that decreased expression of stathmins ameliorates neuromuscular defects (Wen et al., 2013). In $SOD1^{G93A}$ mice, *Stmn1* and *Stmn2* are upregulated at presymptomatic stage, which can contribute to the loss of microtubules and Golgi fragmentation in MN (Bellouze et al., 2016). Following AAV-miR SOD1 gene therapy, the observed downregulation of Stathmin mRNA expression at day 65 indicates that microtubule stabilization may benefit MN at presymptomatic stage of the disease induced by mutated SOD1, possibly limiting the retraction of axons and facilitating the formation of new branches (Poulain & Sobel, 2007). However, previous studies have shown that Stmn2 downregulation also contributes to neurodegeneration in ALS, in particular via the regulatory role of TDP-43 (Klim et al., 2019; Melamed et al., 2019). TDP-43 binds Stmn2 pre-mRNA to prevent alternative splicing of a cryptic exon which generates a premature stop codon and polyadenylation (Klim et al., 2019; Melamed et al., 2019). Therefore, the loss of nuclear TDP-43 associated with ALS and frontotemporal dementia leads to the production a nonfunctional truncated protein and the loss of normal STMN2 expression (Prudencio et al., 2020). Furthermore, STMN2 overexpression induces axonal regeneration in iPSC-derived MN following TDP-43 knockdown (Melamed et al., 2019). These results highlight the multiple roles of Stathmins in the degeneration and regeneration of MN axons, which are not only controlled at transcriptional level, but also by other factors such as autophagic activity, post-translational modifications and interaction with STAT3 (He et al., 2016; Ng et al., 2006; Watabe-Uchida et al., 2006).

We found that the treatment affects the expression of other microtubule-associated proteins in MN. There is a significant downregulation of the *Mapt* gene, which has previously been associated to the risk of developing sporadic ALS (Karch et al., 2018; Sundar et al., 2007). Changes in the expression level of the microtubule-binding tau protein affect cytoskeleton dynamics, via mechanisms controlling the formation of long labile microtubule domains and the organization of microtubules into stable bundles (Baas & Qiang, 2019; Qiang et al., 2018). Upregulation of the kinesin-8 family members *Kif18a* and *Kif18b*, two molecular motors with microtubule-depolymerizing activity, may further control axon length (Kevenaar et al., 2016). Remarkably, transcriptomic analysis also reveals changes related to the post-translational modifications of tubulin. The transcriptional downregulation of *Atat1* (alpha tubulin acetyltransferase 1), an enzyme controlling α-tubulin acetylation, may facilitate axonal branching (Wei et al., 2018). Atat1 also negatively regulates microtubule stability independently from its activity on tubulin acetylation (Kalebic et al., 2013). Overall, the transcriptional changes in MN reveal that the AAV-miR SOD1 treatment may contribute to changes in the cytoskeletal network at this early stage of the SOD1-induced pathology. The observed changes are consistent with enhanced microtubule stability (*Stmn*, *Kif18*, *Atat1*) opposing the hyperdynamic microtubule phenotype previously found in $SOD1^{G93A}$ mice (Fanara et al., 2007), whereas other transcriptional

effects (*Mapt*, *Atat1*) indicate microtubule re-organization possibly facilitating neuronal plasticity.

Unexpectedly, transcription of the neuroprotective factor *Bdnf* was found to be downregulated in ALS mice treated with AAV-miR SOD1. Recently, the role of BDNF in ALS has been debated as this neurotrophic factor may also enhance MN death by increasing glutamate excitotoxicity (Mojsilovic-Petrovic et al., 2006; Pradhan et al., 2019). *Bdnf* downregulation could be an adaptation of lower MN as part of their activity in the motor circuit. Of note, the expression of the proteolytic enzyme Furin is upregulated, which may facilitate the activity-dependent stabilization of NMJ via the processing of mature Bdnf (Je et al., 2013; Seidah et al., 1996).

Overall, the use of AAV-based therapy targeting astrocytes as a platform to silence mSOD1 in the motor system of *SOD1*^{G93A} ALS mice enhances the ability of MN to maintain functional connections with muscle fibers. These effects are particularly evident in the pool of fast-fatigable MN innervating fast-twitch type IIB muscle fibers, which are the most vulnerable to ALS. In the present study, gene therapy targeting mSOD1 was injected to neonatal ALS mice and therefore covered the entire course of the disease. Of note, in a previous report, we also observed a significant albeit more partial protection of the motor function following intrathecal injection of the same astrocyte-targeting AAV-miR SOD1 vector in young adult ALS mice (Dirren et al., 2015), at the time fast-fatigable MN start to degenerate. Overall, these results indicate that astrocyte-targeting gene therapy can slow down ALS progression. When considering its application towards later stages of SOD1-linked ALS, this approach could effectively complement neuroprotective treatments by facilitating muscle reinnervation.

ACKNOWLEDGMENTS

The Authors would like to thank Philippe Colin and Christel Voize for their technical support. We also thank Aline Aebi, Fabienne Pidoux and Viviane Padrun for the technical support and production of viral vectors used in the present study; Valérie Vilmont for editing the manuscript; Mylène Docquier and the Institute of Genetics and Genomics of Geneva (iGE3; http://www.ige3.unige.ch/genomics-platform.php) for high-throughput DNA sequencing. This work was supported by Swiss National Science Foundation grant (310030L_156460/1) and by ERA-NET E-Rare-2 FaSMALS (Grant 3ER30_160673). This research work was also in part supported by a generous donation from Drs Paul and Christa Plichta to honor Mr Boris Canessa. Open access funding provided by Ecole Polytechnique Federale de Lausanne.

CONFLICT OF INTEREST

Cylia Rochat and Bernard Schneider declare a filed patent (WO2017013252A1) entitled "Bicistronic AAV vector for RNA interference in ALS". The other authors declare no competing interests.

AUTHOR CONTRIBUTIONS

Conceptualization: Cylia Rochat, Nathalie Bernard-Marissal, Cédric Raoul, Florence Perrin and Bernard Schneider; Methodology: Cylia Rochat, Florence Perrin, Sylvain Pradervand and Bernard Schneider; Investigation, Cylia Rochat, Nathalie Bernard-Marissal, Florence Perrin and Sylvain Pradervand; Writing–Original Draft, Cylia Rochat, Nathalie Bernard-Marissal and Bernard Schneider; Writing–Review & Editing, Cédric Raoul; Funding Acquisition, Cédric Raoul, Florence Perrin, Patrick Aebischer and Bernard Schneider; Supervision, Bernard Schneider.

DATA AVAILABILITY STATEMENT

The data that support the findings of this study are available from the corresponding author upon reasonable request. The set of RNA sequencing data is available through GEO with ID GSE148901.

ORCID

Emma Källstig https://orcid.org/0000-0002-2282-5690
Florence E. Perrin https://orcid.org/0000-0002-7630-0515
Cédric Raoul https://orcid.org/0000-0003-0561-6851
Bernard L. Schneider https://orcid.org/0000-0001-5485-8748

REFERENCES

Aebischer, J., Cassina, P., Otsmane, B., Moumen, A., Seilhean, D., Meininger, V., Barbeito, L., Pettmann, B., & Raoul, C. (2011). IFNγ triggers a LIGHT-dependent selective death of motoneurons contributing to the non-cell-autonomous effects of mutant SOD1. *Cell Death and Differentiation*, *18*(5), 754–768. https://doi.org/10.1038/cdd.2010.143

Anders, S., Pyl, P. T., & Huber, W. (2015). HTSeq—A python framework to work with high-throughput sequencing data. *Bioinformatics*, *31*(2), 166–169. https://doi.org/10.1093/bioinformatics/btu638

Anneser, J. M. H., Cookson, M. R., Ince, P. G., Shaw, P. J., & Borasio, G. D. (2001). Glial cells of the spinal cord and subcortical white matter upregulate neuronal nitric oxide synthase in sporadic amyotrophic lateral sclerosis. *Experimental Neurology*, *171*(2), 418–421. https://doi.org/10.1006/exnr.2001.7756

Baas, P. W., & Qiang, L. (2019). Tau: It's not what you think. *Trends in Cell Biology*, *29*(6), 452–461. https://doi.org/10.1016/j.tcb.2019.02.007

Baloh, R. H., Rakowicz, W., Gardner, R., & Pestronk, A. (2007). Frequent atrophic groups with mixed-type myofibers is distinctive to motor neuron syndromes. *Muscle & Nerve*, *36*(1), 107–110. https://doi.org/10.1002/mus.20755

Beers, D. R., Henkel, J. S., Xiao, Q., Zhao, W., Wang, J., Yen, A. A., Siklos, L., McKercher, S. R., & Appel, S. H. (2006). Wild-type microglia extend survival in PU.1 knockout mice with familial amyotrophic lateral sclerosis. *Proceedings of the National Academy of Sciences USA*, *103*(43), 16021–16026. https://doi.org/10.1073/pnas.0607423103

Bellouze, S., Baillat, G., Buttigieg, D., De la Grange, P., Rabouille, C., & Haase, G. (2016). Stathmin 1/2-triggered microtubule loss mediates Golgi fragmentation in mutant SOD1 motor neurons. *Molecular Neurodegeneration*, *11*(1), 43. https://doi.org/10.1186/s13024-016-0111-6

Bi, F., Huang, C., Tong, J., Qiu, G., Huang, B., Wu, Q., Li, F., Xu, Z., Bowser, R., Xia, X. G., & Zhou, H. (2013). Reactive astrocytes secrete lcn2 to promote neuron death. *Proceedings of the National Academy of Sciences USA*, *110*(10), 4069–4074. https://doi.org/10.1073/pnas.1218497110

Blakely, P. K., Hussain, S., Carlin, L. E., & Irani, D. N. (2015). Astrocyte matricellular proteins that control excitatory synaptogenesis are regulated by inflammatory cytokines and correlate with paralysis severity during experimental autoimmune encephalomyelitis. *Frontiers in Neuroscience*, *9*, 344. https://doi.org/10.3389/fnins.2015.00344

Boillee, S., Yamanaka, K., Lobsiger, C. S., Copeland, N. G., Jenkins, N. A., Kassiotis, G., Kollias, G., & Cleveland, D. W. (2006). Onset and progression in inherited ALS determined by motor neurons and microglia. *Science*, *312*(5778), 1389–1392. https://doi.org/10.1126/science.1123511

Catania, M. V., Aronica, E., Yankaya, B., & Troost, D. (2001). Increased expression of neuronal nitric oxide synthase spliced variants in

reactive astrocytes of amyotrophic lateral sclerosis human spinal cord. *The Journal of Neuroscience*, *21*(11), RC148.

Chauvin, S., & Sobel, A. (2015). Neuronal stathmins: A family of phosphoproteins cooperating for neuronal development, plasticity and regeneration. *Progress in Neurobiology*, *126*, 1–18. https://doi.org/10.1016/j.pneurobio.2014.09.002

Christopherson, K. S., Ullian, E. M., Stokes, C. C. A., Mullowney, C. E., Hell, J. W., Agah, A., Lawler, J., Mosher, D. F., Bornstein, P., & Barres, B. A. (2005). Thrombospondins are astrocyte-secreted proteins that promote CNS synaptogenesis. *Cell*, *120*(3), 421–433. https://doi.org/10.1016/j.cell.2004.12.020

Clarke, L. E., & Barres, B. A. (2013). Emerging roles of astrocytes in neural circuit development. *Nature Reviews Neuroscience*, *14*(5), 311–321. https://doi.org/10.1038/nrn3484

Damme, P. V., Bogaert, E., Dewil, M., Hersmus, N., Kiraly, D., Scheveneels, W., Bockx, I., Braeken, D., Verpoorten, N., Verhoeven, K., Timmerman, V., Herijgers, P., Callewaert, G., Carmeliet, P., Bosch, L. V. D., & Robberecht, W. (2007). Astrocytes regulate GluR2 expression in motor neurons and their vulnerability to excitotoxicity. *Proceedings of the National Academy of Sciences USA*, *104*(37), 14825–14830. https://doi.org/10.1073/pnas.0705046104

Davis, M. P. A., van Dongen, S., Abreu-Goodger, C., Bartonicek, N., & Enright, A. J. (2013). Kraken: A set of tools for quality control and analysis of high-throughput sequence data. *Methods (San Diego, Calif.)*, *63*(1), 41–49. https://doi.org/10.1016/j.ymeth.2013.06.027

Delestrée, N., Manuel, M., Iglesias, C., Elbasiouny, S. M., Heckman, C. J., & Zytnicki, D. (2014). Adult spinal motoneurones are not hyperexcitable in a mouse model of inherited amyotrophic lateral sclerosis. *The Journal of Physiology*, *592*(Pt 7), 1687–1703. https://doi.org/10.1113/jphysiol.2013.265843

Dirren, E., Aebischer, J., Rochat, C., Towne, C., Schneider, B. L., & Aebischer, P. (2015). SOD1 silencing in motoneurons or glia rescues neuromuscular function in ALS mice. *Annals of Clinical and Translational Neurology*, *2*(2), 167–184. https://doi.org/10.1002/acn3.162

Dirren, E., Towne, C. L., Setola, V., Redmond, D. E., Schneider, B. L., & Aebischer, P. (2014). Intracerebroventricular injection of adeno-associated virus 6 and 9 vectors for cell type-specific transgene expression in the spinal cord. *Human Gene Therapy*, *25*(2), 109–120. https://doi.org/10.1089/hum.2013.021

Dobin, A., Davis, C. A., Schlesinger, F., Drenkow, J., Zaleski, C., Jha, S., Batut, P., Chaisson, M., & Gingeras, T. R. (2013). STAR: Ultrafast universal RNA-seq aligner. *Bioinformatics*, *29*(1), 15–21. https://doi.org/10.1093/bioinformatics/bts635

Eden, E., Navon, R., Steinfeld, I., Lipson, D., & Yakhini, Z. (2009). GOrilla: A tool for discovery and visualization of enriched GO terms in ranked gene lists. *BMC Bioinformatics*, *10*(1), 48. https://doi.org/10.1186/1471-2105-10-48

Endo, F., Komine, O., Fujimori-Tonou, N., Katsuno, M., Jin, S., Watanabe, S., Sobue, G., Dezawa, M., Wyss-Coray, T., & Yamanaka, K. (2015). Astrocyte-derived TGF-β1 accelerates disease progression in ALS mice by interfering with the Neuroprotective functions of microglia and T cells. *Cell Reports*, *11*(4), 592–604. https://doi.org/10.1016/j.celrep.2015.03.053

Fanara, P., Banerjee, J., Hueck, R. V., Harper, M. R., Awada, M., Turner, H., Husted, K. H., Brandt, R., & Hellerstein, M. K. (2007). Stabilization of Hyperdynamic microtubules is Neuroprotective in amyotrophic lateral sclerosis. *Journal of Biological Chemistry*, *282*(32), 23465–23472. https://doi.org/10.1074/jbc.M703434200

Feng, Z., & Ko, C.-P. (2008). Schwann cells promote synaptogenesis at the neuromuscular junction via transforming growth factor-β1. *The Journal of Neuroscience*, *28*(39), 9599–9609. https://doi.org/10.1523/JNEUROSCI.2589-08.2008

Ferraiuolo, L., Higginbottom, A., Heath, P. R., Barber, S., Greenald, D., Kirby, J., & Shaw, P. J. (2011). Dysregulation of astrocyte-motoneuron cross-talk in mutant superoxide dismutase 1-related amyotrophic lateral sclerosis. *Brain*, *134*(Pt 9), 2627–2641. https://doi.org/10.1093/brain/awr193

Foust, K. D., Salazar, D. L., Likhite, S., Ferraiuolo, L., Ditsworth, D., Ilieva, H., Meyer, K., Schmelzer, L., Braun, L., Cleveland, D. W., & Kaspar, B. K. (2013). Therapeutic AAV9-mediated suppression of mutant SOD1 slows disease progression and extends survival in models of inherited ALS. *Molecular Therapy*, *21*(12), 2148–2159. https://doi.org/10.1038/mt.2013.211

Frey, D., Schneider, C., Xu, L., Borg, J., Spooren, W., & Caroni, P. (2000). Early and selective loss of neuromuscular synapse subtypes with low sprouting competence in motoneuron diseases. *The Journal of Neuroscience*, *20*(7), 2534–2542.

Fuentes-Medel, Y., Logan, M. A., Ashley, J., Ataman, B., Budnik, V., & Freeman, M. R. (2009). Glia and muscle sculpt neuromuscular arbors by engulfing destabilized synaptic Boutons and shed presynaptic debris. *PLoS Biology*, *7*(8), e1000184. https://doi.org/10.1371/journal.pbio.1000184

Gharbi, T., Zhang, Z., & Yang, G.-Y. (2020). The function of astrocyte mediated extracellular vesicles in central nervous system diseases. *Frontiers in Cell and Developmental Biology*, *8*, 1135. https://doi.org/10.3389/fcell.2020.568889

Gordon, T., Tyreman, N., Li, S., Putman, C. T., & Hegedus, J. (2010). Functional over-load saves motor units in the SOD1-G93A transgenic mouse model of amyotrophic lateral sclerosis. *Neurobiology of Disease*, *37*(2), 412–422. https://doi.org/10.1016/j.nbd.2009.10.021

Griffin, J. M., Fackelmeier, B., Fong, D. M., Mouravlev, A., Young, D., & O'Carroll, S. J. (2019). Astrocyte-selective AAV gene therapy through the endogenous GFAP promoter results in robust transduction in the rat spinal cord following injury. *Gene Therapy*, *26*(5), 198–210. https://doi.org/10.1038/s41434-019-0075-6

Gurney, M. E., Pu, H., Chiu, A. Y., Dal Canto, M. C., Polchow, C. Y., Alexander, D. D., Caliendo, J., Hentati, A., Kwon, Y. W., Deng, H. X., et al. (1994). Motor neuron degeneration in mice that express a human cu,Zn superoxide dismutase mutation. *Science*, *264*(5166), 1772–1775.

Guttenplan, K. A., Weigel, M. K., Adler, D. I., Couthouis, J., Liddelow, S. A., Gitler, A. D., & Barres, B. A. (2020). Knockout of reactive astrocyte activating factors slows disease progression in an ALS mouse model. *Nature Communications*, *11*(1), 3753. https://doi.org/10.1038/s41467-020-17514-9

Haenold, R., Weih, F., Herrmann, K.-H., Schmidt, K.-F., Krempler, K., Engelmann, C., Nave, K.-A., Reichenbach, J. R., Lowel, S., Witte, O. W., & Kretz, A. (2014). NF-kB controls axonal regeneration and degeneration through cell-specific balance of RelA and p50 in the adult CNS. *Development*, *141*(15), e1505. https://doi.org/10.1242/dev.115097

Haidet-Phillips, A. M., Hester, M. E., Miranda, C. J., Meyer, K., Braun, L., Frakes, A., Song, S., Likhite, S., Murtha, M. J., Foust, K. D., Rao, M., Eagle, A., Kammesheidt, A., Christensen, A., Mendell, J. R., Burghes, A. H., & Kaspar, B. K. (2011). Astrocytes from familial and sporadic ALS patients are toxic to motor neurons. *Nature Biotechnology*, *29*(9), 824–828. https://doi.org/10.1038/nbt.1957

Harrison, J. M., & Rafuse, V. F. (2020). Muscle fiber-type specific terminal Schwann cell pathology leads to sprouting deficits following partial denervation in SOD1G93A mice. *Neurobiology of Disease*, *145*, 105052. https://doi.org/10.1016/j.nbd.2020.105052

He, M., Ding, Y., Chu, C., Tang, J., Xiao, Q., & Luo, Z.-G. (2016). Autophagy induction stabilizes microtubules and promotes axon regeneration after spinal cord injury. *Proceedings of the National Academy of Sciences USA*, *113*(40), 11324–11329. https://doi.org/10.1073/pnas.1611282113

Hol, E. M., Roelofs, R. F., Moraal, E., Sonnemans, M., Sluijs, J. A., Proper, E. A., de Graan, P. N. E., Fischer, D. F., & van Leeuwen, F. W. (2003). Neuronal expression of GFAP in patients with Alzheimer pathology and identification of novel GFAP splice forms. *Molecular Psychiatry*, *8*(9), 786–796. https://doi.org/10.1038/sj.mp.4001379

Je, H. S., Yang, F., Ji, Y., Potluri, S., Fu, X.-Q., Luo, Z.-G., Nagappan, G., Chan, J. P., Hempstead, B., Son, Y.-J., & Lu, B. (2013). ProBDNF and mature BDNF as punishment and reward signals for synapse elimination at mouse neuromuscular junctions. *The Journal of Neuroscience*, *33*(24), 9957–9962. https://doi.org/10.1523/JNEUROSCI.0163-13.2013

Jokela, M., Huovinen, S., Raheem, O., Lindfors, M., Palmio, J., Penttila, S., & Udd, B. (2016). Distinct muscle biopsy findings in genetically defined adult-onset motor neuron disorders. *PLoS One*, *11*(3), e0151376. https://doi.org/10.1371/journal.pone.0151376

Kalebic, N., Martinez, C., Perlas, E., Hublitz, P., Bilbao-Cortes, D., Fiedorczuk, K., Andolfo, A., & Heppenstall, P. A. (2013). Tubulin Acetyltransferase αTAT1 destabilizes microtubules independently of its acetylation activity. *Molecular and Cellular Biology*, *33*(6), 1114–1123. https://doi.org/10.1128/MCB.01044-12

Kang, S. H., Li, Y., Fukaya, M., Lorenzini, I., Cleveland, D. W., Ostrow, L. W., Rothstein, J. D., & Bergles, D. E. (2013). Degeneration and impaired regeneration of gray matter oligodendrocytes in amyotrophic lateral sclerosis. *Nature Neuroscience*, *16*(5), 571–579. https://doi.org/10.1038/nn.3357

Kaplan, A., Spiller, K. J., Towne, C., Kanning, K. C., Choe, G. T., Geber, A., Akay, T., Aebischer, P., & Henderson, C. E. (2014). Neuronal matrix metalloproteinase-9 is a determinant of selective neurodegeneration. *Neuron*, *81*(2), 333–348. https://doi.org/10.1016/j.neuron.2013.12.009

Karch, C. M., Wen, N., Fan, C. C., Yokoyama, J. S., Kouri, N., Ross, O. A., Höglinger, G., Müller, U., Ferrari, R., Hardy, J., Schellenberg, G. D., Sleiman, P. M., Momeni, P., Hess, C. P., Miller, B. L., Sharma, M., Deerlin, V. V., Smeland, O. B., Andreassen, O. A., … Desikan, R. S. (2018). Selective genetic overlap between amyotrophic lateral sclerosis and diseases of the Frontotemporal dementia Spectrum. *JAMA Neurology*, *75*(7), 860–875. https://doi.org/10.1001/jamaneurol.2018.0372

Kevenaar, J. T., Bianchi, S., van Spronsen, M., Olieric, N., Lipka, J., Frias, C. P., Mikhaylova, M., Harterink, M., Keijzer, N., Wulf, P. S., Hilbert, M., Kapitein, L. C., de Graaff, E., Ahkmanova, A., Steinmetz, M. O., & Hoogenraad, C. C. (2016). Kinesin-binding protein controls microtubule dynamics and cargo trafficking by regulating Kinesin motor activity. *Current Biology*, *26*(7), 849–861. https://doi.org/10.1016/j.cub.2016.01.048

Klim, J. R., Williams, L. A., Limone, F., Juan, I. G. S., Davis-Dusenbery, B. N., Mordes, D. A., Burberry, A., Steinbaugh, M. J., Gamage, K. K., Kirchner, R., Moccia, R., Cassel, S. H., Chen, K., Wainger, B. J., Woolf, C. J., & Eggan, K. (2019). ALS-implicated protein TDP-43 sustains levels of STMN2, a mediator of motor neuron growth and repair. *Nature Neuroscience*, *22*(2), 167–179. https://doi.org/10.1038/s41593-018-0300-4

Kondo, T., Funayama, M., Tsukita, K., Hotta, A., Yasuda, A., Nori, S., Kaneko, S., Nakamura, M., Takahashi, R., Okano, H., Yamanaka, S., & Inoue, H. (2014). Focal transplantation of human iPSC-derived glial-rich neural progenitors improves lifespan of ALS mice. *Stem Cell Reports*, *3*(2), 242–249. https://doi.org/10.1016/j.stemcr.2014.05.017

Kucukdereli, H., Allen, N. J., Lee, A. T., Feng, A., Ozlu, M. I., Conatser, L. M., Chakraborty, C., Workman, G., Weaver, M., Sage, E. H., Barres, B. A., & Eroglu, C. (2011). Control of excitatory CNS synaptogenesis by astrocyte-secreted proteins Hevin and SPARC. *Proceedings of the National Academy of Sciences USA*, *108*(32), E440–E449. https://doi.org/10.1073/pnas.1104977108

Lepore, A. C., Rauck, B., Dejea, C., Pardo, A. C., Rao, M. S., Rothstein, J. D., & Maragakis, N. J. (2008). Focal transplantation-based astrocyte replacement is neuroprotective in a model of motor neuron disease. *Nature Neuroscience*, *11*(11), 1294–1301. https://doi.org/10.1038/nn.2210

Li, B., & Dewey, C. N. (2011). RSEM: Accurate transcript quantification from RNA-Seq data with or without a reference genome. *BMC Bioinformatics*, *12*(1), 323. https://doi.org/10.1186/1471-2105-12-323

Love, M. I., Huber, W., & Anders, S. (2014). Moderated estimation of fold change and dispersion for RNA-seq data with DESeq2. *Genome Biology*, *15*(12), 550. https://doi.org/10.1186/s13059-014-0550-8

Martin, M. (2011). Cutadapt removes adapter sequences from high-throughput sequencing reads. *EMBnet.Journal*, *17*(1), 10–12. https://doi.org/10.14806/ej.17.1.200

Martínez-Silva, M. d. L., Imhoff-Manuel, R. D., Sharma, A., Heckman, C., Shneider, N. A., Roselli, F., Zytnicki, D., & Manuel, M. (2018). Hypoexcitability precedes denervation in the large fast-contracting motor units in two unrelated mouse models of ALS. *eLife*, *7*, e30955. https://doi.org/10.7554/eLife.30955

McCampbell, A., Cole, T., Wegener, A. J., Tomassy, G. S., Setnicka, A., Farley, B. J., Schoch, K. M., Hoye, M. L., Shabsovich, M., Sun, L., Luo, Y., Zhang, M., Comfort, N., Wang, B., Amacker, J., Thankamony, S., Salzman, D. W., Cudkowicz, M., Graham, D. L., … Miller, T. M. (2018). Antisense oligonucleotides extend survival and reverse decrement in muscle response in ALS models. *The Journal of Clinical Investigation*, *128*(8), 3558–3567. https://doi.org/10.1172/JCI99081

Melamed, Z., López-Erauskin, J., Baughn, M. W., Zhang, O., Drenner, K., Sun, Y., Freyermuth, F., McMahon, M. A., Beccari, M. S., Artates, J. W., Ohkubo, T., Rodriguez, M., Lin, N., Wu, D., Bennett, C. F., Rigo, F., Cruz, S. D., Ravits, J., Lagier-Tourenne, C., & Cleveland, D. W. (2019). Premature polyadenylation-mediated loss of stathmin-2 is a hallmark of TDP-43-dependent neurodegeneration. *Nature Neuroscience*, *22*(2), 180–190. https://doi.org/10.1038/s41593-018-0293-z

Mojsilovic-Petrovic, J., Jeong, G.-B., Crocker, A., Arneja, A., David, S., Russell, D., & Kalb, R. G. (2006). Protecting motor neurons from toxic insult by antagonism of adenosine A2a and Trk receptors. *The Journal of Neuroscience*, *26*(36), 9250–9263. https://doi.org/10.1523/JNEUROSCI.1856-06.2006

Nagai, M., Re, D. B., Nagata, T., Chalazonitis, A., Jessell, T. M., Wichterle, H., & Przedborski, S. (2007). Astrocytes expressing ALS-linked mutated SOD1 release factors selectively toxic to motor neurons. *Nature Neuroscience*, *10*(5), 615–622. https://doi.org/10.1038/nn1876

Ng, D. C. H., Lin, B. H., Lim, C. P., Huang, G., Zhang, T., Poli, V., & Cao, X. (2006). Stat3 regulates microtubules by antagonizing the depolymerization activity of stathmin. *Journal of Cell Biology*, *172*(2), 245–257. https://doi.org/10.1083/jcb.200503021

Nishizawa, T., Yamashia, S., McGrath, K. F., Tamaki, H., Kasuga, N., & Takekura, H. (2006). Plasticity of neuromuscular junction architectures in rat slow and fast muscle fibers following temporary denervation and reinnervation processes. *Journal of Muscle Research and Cell Motility*, *27*(8), 607–615. https://doi.org/10.1007/s10974-006-9094-1

Papadeas, S. T., Kraig, S. E., O'Banion, C., Lepore, A. C., & Maragakis, N. J. (2011). Astrocytes carrying the superoxide dismutase 1 (SOD1G93A) mutation induce wild-type motor neuron degeneration in vivo. *Proceedings of the National Academy of Sciences USA*, *108*(43), 17803–17808. https://doi.org/10.1073/pnas.1103141108

Poulain, F. E., & Sobel, A. (2007). The "SCG10-LIke protein" SCLIP is a novel regulator of axonal branching in hippocampal neurons, unlike SCG10. *Molecular and Cellular Neuroscience*, *34*(2), 137–146. https://doi.org/10.1016/j.mcn.2006.10.012

Pradhan, J., Noakes, P. G., & Bellingham, M. C. (2019). The role of altered BDNF/TrkB signaling in amyotrophic lateral sclerosis. *Frontiers in Cellular Neuroscience*, *13*, 368. https://doi.org/10.3389/fncel.2019.00368

Pramatarova, A., Laganiere, J., Roussel, J., Brisebois, K., & Rouleau, G. A. (2001). Neuron-specific expression of mutant superoxide dismutase 1 in transgenic mice does not lead to motor impairment. *The Journal of Neuroscience*, *21*(10), 3369–3374.

Prudencio, M., Humphrey, J., Pickles, S., Brown, A.-L., Hill, S. E., Kachergus, J. M., Shi, J., Heckman, M. G., Spiegel, M. R., Cook, C., Song, Y., Yue, M., Daughrity, L. M., Carlomagno, Y., Jansen-West, K., De Castro, C. F., DeTure, M., Koga, S., Wang, Y.-C., … Petrucelli, L.

(2020). Truncated stathmin-2 is a marker of TDP-43 pathology in frontotemporal dementia. *The Journal of Clinical Investigation*, *130*(11), 6080–6092. https://doi.org/10.1172/JCI139741

Pun, S., Santos, A. F., Saxena, S., Xu, L., & Caroni, P. (2006). Selective vulnerability and pruning of phasic motoneuron axons in motoneuron disease alleviated by CNTF. *Nature Neuroscience*, *9*(3), 408–419. https://doi.org/10.1038/nn1653

Qiang, L., Sun, X., Austin, T. O., Muralidharan, H., Jean, D. C., Liu, M., Yu, W., & Baas, P. W. (2018). Tau does not stabilize axonal microtubules but rather enables them to have long labile domains. *Current Biology*, *28*(13), 2181–2189.e4. https://doi.org/10.1016/j.cub.2018.05.045

Ralph, G. S., Radcliffe, P. A., Day, D. M., Carthy, J. M., Leroux, M. A., Lee, D. C., Wong, L. F., Bilsland, L. G., Greensmith, L., Kingsman, S. M., Mitrophanous, K. A., Mazarakis, N. D., & Azzouz, M. (2005). Silencing mutant SOD1 using RNAi protects against neurodegeneration and extends survival in an ALS model. *Nature Medicine*, *11*(4), 429–433. https://doi.org/10.1038/nm1205

Ramírez-Jarquín, U. N., Rojas, F., Van Zundert, B., & Tapia, R. (2017). Chronic infusion of SOD1G93A astrocyte-secreted factors induces spinal motoneuron degeneration and neuromuscular dysfunction in healthy rats. *Journal of Cellular Physiology*, *232*(10), 2610–2615. https://doi.org/10.1002/jcp.25827

Raoul, C., Abbas-Terki, T., Bensadoun, J. C., Guillot, S., Haase, G., Szulc, J., Henderson, C. E., & Aebischer, P. (2005). Lentiviral-mediated silencing of SOD1 through RNA interference retards disease onset and progression in a mouse model of ALS. *Nature Medicine*, *11*(4), 423–428. https://doi.org/10.1038/nm1207

Rojas, F., Cortes, N., Abarzua, S., Dyrda, A., & Van Zundert, B. (2014). Astrocytes expressing mutant SOD1 and TDP43 trigger motoneuron death that is mediated via sodium channels and nitroxidative stress. *Frontiers in Cellular Neuroscience*, *8*, 24. https://doi.org/10.3389/fncel.2014.00024

Rothstein, J. D., Van Kammen, M., Levey, A. I., Martin, L. J., & Kuncl, R. W. (1995). Selective loss of glial glutamate transporter GLT-1 in amyotrophic lateral sclerosis. *Annals of Neurology*, *38*(1), 73–84. https://doi.org/10.1002/ana.410380114

Schaefer, A. M., Sanes, J. R., & Lichtman, J. W. (2005). A compensatory subpopulation of motor neurons in a mouse model of amyotrophic lateral sclerosis. *Journal of Comparative Neurology*, *490*(3), 209–219. https://doi.org/10.1002/cne.20620

Seidah, N. G., Benjannet, S., Pareek, S., Chrétien, M., & Murphy, R. A. (1996). Cellular processing of the neurotrophin precursors of NT3 and BDNF by the mammalian proprotein convertases. *FEBS Letters*, *379*(3), 247–250. https://doi.org/10.1016/0014-5793(95)01520-5

Spiller, K. J., Cheung, C. J., Restrepo, C. R., Kwong, L. K., Stieber, A. M., Trojanowski, J. Q., & Lee, V. M.-Y. (2016). Selective motor neuron resistance and recovery in a new inducible mouse model of TDP-43 Proteinopathy. *The Journal of Neuroscience*, *36*(29), 7707–7717. https://doi.org/10.1523/JNEUROSCI.1457-16.2016

Stoica, L., Todeasa, S. H., Cabrera, G. T., Salameh, J. S., ElMallah, M. K., Mueller, C., Brown, R. H., & Miguel, S.-E. (2016). AAV delivered artificial microRNA extends survival and delays paralysis in an amyotrophic lateral sclerosis mouse model. *Annals of Neurology*, *79*(4), 687–700. https://doi.org/10.1002/ana.24618

Sundar, P. D., Yu, C.-E., Sieh, W., Steinbart, E., Garruto, R. M., Oyanagi, K., Craig, U.-K., Bird, T. D., Wijsman, E. M., Galasko, D. R., & Schellenberg, G. D. (2007). Two sites in the MAPT region confer genetic risk for Guam ALS/PDC and dementia. *Human Molecular Genetics*, *16*(3), 295–306. https://doi.org/10.1093/hmg/ddl463

Taschenberger, G., Tereshchenko, J., & Kügler, S. (2017). A MicroRNA124 target sequence restores astrocyte specificity of gfaABC1D-driven transgene expression in AAV-mediated gene transfer. *Molecular Therapy. Nucleic Acids*, *8*, 13–25. https://doi.org/10.1016/j.omtn.2017.03.009

Taylor, J. P., Brown, R. H., & Cleveland, D. W. (2016). Decoding ALS: From genes to mechanism. *Nature*, *539*(7628), 197–206. https://doi.org/10.1038/nature20413

Tripathi, P., Rodriguez-Muela, N., Klim, J. R., De Boer, A. S., Agrawal, S., Sandoe, J., Lopes, C. S., Ogliari, K. S., Williams, L. A., Shear, M., Rubin, L. L., Eggan, K., & Zhou, Q. (2017). Reactive astrocytes promote ALS-like degeneration and intracellular protein aggregation in human motor neurons by disrupting autophagy through TGF-β1. *Stem Cell Reports*, *9*(2), 667–680. https://doi.org/10.1016/j.stemcr.2017.06.008

Ullian, E. M., Harris, B. T., Wu, A., Chan, J. R., & Barres, B. A. (2004). Schwann cells and astrocytes induce synapse formation by spinal motor neurons in culture. *Molecular and Cellular Neuroscience*, *25*(2), 241–251. https://doi.org/10.1016/j.mcn.2003.10.011

Wang, L., Wang, S., & Li, W. (2012). RSeQC: Quality control of RNA-seq experiments. *Bioinformatics*, *28*(16), 2184–2185. https://doi.org/10.1093/bioinformatics/bts356

Watabe-Uchida, M., John, K. A., Janas, J. A., Newey, S. E., & Van Aelst, L. (2006). The Rac activator DOCK7 regulates neuronal polarity through local phosphorylation of Stathmin/Op18. *Neuron*, *51*(6), 727–739. https://doi.org/10.1016/j.neuron.2006.07.020

Wei, D., Gao, N., Li, L., Zhu, J.-X., Diao, L., Huang, J., Han, Q.-J., Wang, S., Xue, H., Wang, Q., Wu, Q.-F., Zhang, X., & Bao, L. (2018). α-Tubulin acetylation restricts axon Overbranching by dampening microtubule plus-end dynamics in neurons. *Cerebral Cortex*, *28*(9), 3332–3346. https://doi.org/10.1093/cercor/bhx225

Wen, H. L., Ting, C. H., Liu, H. C., Li, H., & Lin-Chao, S. (2013). Decreased stathmin expression ameliorates neuromuscular defects but fails to prolong survival in a mouse model of spinal muscular atrophy. *Neurobiology of Disease*, *52*, 94–103. https://doi.org/10.1016/j.nbd.2012.11.015

Winter, F. D., Vo, T., Stam, F. J., Wisman, L. A. B., Bär, P. R., Niclou, S. P., van Muiswinkel, F. L., & Verhaagen, J. (2006). The expression of the chemorepellent Semaphorin 3A is selectively induced in terminal Schwann cells of a subset of neuromuscular synapses that display limited anatomical plasticity and enhanced vulnerability in motor neuron disease. *Molecular and Cellular Neuroscience*, *32*(1), 102–117. https://doi.org/10.1016/j.mcn.2006.03.002

Yamanaka, K., Boillee, S., Roberts, E. A., Garcia, M. L., McAlonis-Downes, M., Mikse, O. R., Cleveland, D. W., & Goldstein, L. S. (2008). Mutant SOD1 in cell types other than motor neurons and oligodendrocytes accelerates onset of disease in ALS mice. *Proceedings of the National Academy of Sciences USA*, *105*(21), 7594–7599. https://doi.org/10.1073/pnas.0802556105

SUPPORTING INFORMATION

Additional supporting information may be found in the online version of the article at the publisher's website.

How to cite this article: Rochat, C., Bernard-Marissal, N., Källstig, E., Pradervand, S., Perrin, F. E., Aebischer, P., Raoul, C., & Schneider, B. L. (2022). Astrocyte-targeting RNA interference against mutated superoxide dismutase 1 induces motoneuron plasticity and protects fast-fatigable motor units in a mouse model of amyotrophic lateral sclerosis. *Glia*, *70*(5), 842–857. https://doi.org/10.1002/glia.24140